Monitoring of Construction Over Soft CCR Deposits

Pedro Amaya[1], Michelle Perez-Canals[1], Mary Nodine[1], Will Lukas[1]

[1] GEI Consultants, Inc., 400 Unicorn Park Drive, Woburn, MA 01801

KEYWORDS: CCR, Deformation, Strain, Creep, Triaxial Test, Direct Shear Test, Deformation Ratio.

ABSTRACT

Compliance with Coal Combustion Residual (CCR) regulations has dictated the need to close CCR impoundments in place, excavate CCR materials from ponds for placement on suitable landfills, or create hybrid facilities where additional CCR materials are placed above the existing level of CCR deposits. All these options lead to loading of soft deposits within a CCR foundation, or to the creation of soft-wet layers within the recently placed CCR materials. Construction over soft layers and deposits is usually done by using a series of assumptions based on limited data during the design, with localized conditions extrapolated to generalize the site. Designs target factors of safety against slope stability failure that reflect successful experiences with similar materials and loading conditions, creating a need for verification of the design by monitoring during the construction and post-construction phases.

Ladd (1991) indicates that Tavenas et al. (1979) demonstrated that correlations between horizontal and vertical displacements provide useful information regarding the importance of undrained versus drained deformations within embankment foundations, thus allowing the recognition of possible failure mechanisms in a timely manner. Vertical and lateral deformations are associated with volumetric changes of soft materials driven by changes in the effective stresses acting on the material.

The authors of this paper describe instances where construction at CCR sites were successfully monitored with a combination of inclinometers, settlement plates or extensometers, and piezometers. Observations of the behavior of pore-water pressure and vertical and horizontal deformations of the soft layers and deposits led to the conclusion that the facilities were performing as intended in the design. Construction at these sites continued past the monitoring period presented in this effort.

1 - INTRODUCTION

Construction over saturated weak deposits is a delicate endeavor. A series of assumptions must be made during design based on limited data representing localized conditions that have been extrapolated into a generalization of the site and a set of expected outcomes. Field instrumentation is generally included in a project to facilitate construction, to validate assumptions made during design, to assess the performance of

the facility during its service life, and/or to fulfill regulatory requirements. However, a framework for monitoring instrumentation to verify the performance of constructions over soft or weak deposits is not readily available as monitoring is often used during the construction process or as forensic tools following a failure.

Often geotechnical engineering advances as we learn about the mechanism that may have taken place in the soil after a failure has occurred. The forensic investigation attempts to establish a connection between what took place, and what it is understood about soil behavior. In the work described herein, the authors attempt to review the behavior of CCR materials as revealed by the records of monitoring construction processes completed without an incident, providing a framework for monitoring the performance of facilities constructed on weak CCR deposits.

II - LITERATURE REVIEW

There is considerable uncertainty in the assessment of stability of embankments on soft ground due to the difficulty in predicting the undrained behavior of soft soil layers. Hunter and Fell (2003) reported that in the work of El-Remley (2001), it was shown that for embankments on soft ground, a factor of safety of 1.5 corresponds to a probability of unsatisfactory performance of about 1 in 50. This is a result of the uncertainty in determining the undrained behavior of the soft soils during the design process. Therefore, to supplement the information gathered during field and laboratory testing programs, instrumentation at a site should be used to provide information on the amount of deformation taking place. By doing this, the associated mobilized strength can be estimated to determine if at any time during construction the soft layers exhibit behaviors that would result in an exceedance of the design shear strength, and therefore allow time to develop and implement remedial actions if necessary.

Deformation

The total settlement of a weak layer under an embankment will be a combination of immediate settlement, consolidation settlement and creep settlement.
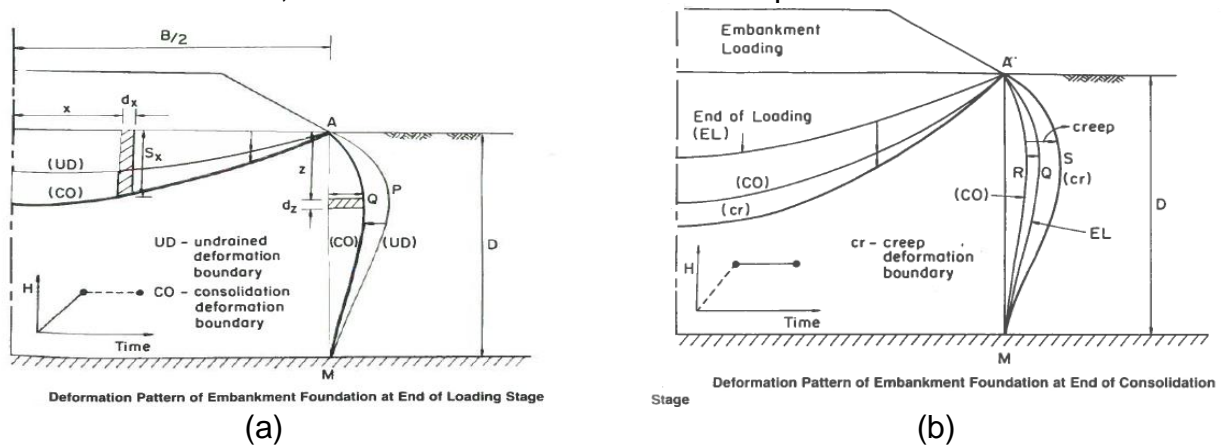

| (a) | (b) |

Figure 1. Deformation of Embankments on soft foundations (a) end of loading stage, (b) end of consolidation stage [adapted after Loganathan, N. et al. (1993) *Deformation Analysis of Embankments.*]

Loganathan, N. et al. (1993) pointed out that during loading and consolidation stages of an embankment considerable volume changes occur in the foundation soil, the magnitude of which depend on the load applied and the duration of consolidation. The volume changes, which occur vertically and laterally, are associated with settlement and lateral deformations of an embankment's foundation. Tavenas et al. (1979) summarized the results of a study of 21 embankments on soft soils. Ladd (1991) indicates that Tavenas et al. (1979) had demonstrated that correlations between horizontal displacements and vertical settlements can provide useful information regarding the relative importance of undrained versus drained deformations within embankment foundations. Ladd (1991) related some of the main points of Tavena et al. 1979 work indicating that the relationship between maximum horizontal displacement (h_m) measured by inclinometers at the toe of the embankment, and the maximum settlement (s) can be used to understand the behavior of the foundation material. Changes in the slope of h_m versus s observed during and after construction, and the shape of the horizontal displacement h_m versus s curves lead to the conclusions listed below. For ease of presentation, the h_m versus s slope is called the deformation ratio, $DR = dh_m/ds.$

a) Significant drainage during initial loading causes horizontal displacements resulting in DR = $dh_m/ds = 0.18$ +/- 0.09 SD

b) A relatively abrupt increase in horizontal displacements occurs when a significant zone of the foundation becomes "normally consolidated," such that undrained shear deformations dominate behavior; DR = $dh_m/ds = 0.9$ +/- 0.2 SD during this phase.

c) The maximum displacement of the h_m versus s curve more or less coincides with the location of the minimum undrained strength within the foundation soil.

After additional consolidation over several years for 12 of the embankments studied, having average embankment width / depth of soft soil, (B/D) ranging from 0.9 to almost 10, it was reported that:

d) The maximum horizontal displacement continues to increase linearly with settlement; DR = $dh_m/ds = 0.16$ +/- 0.07SD and can be affected by small changes in slope geometry.

e) The h_m versus s shape remains approximately constant unless the thickness of normally consolidated soil increases with time.

Similarly, Walton (2017) indicated that in his work at fly ash facilities, he had achieved construction success while maintaining $h_m/s \approx 0.2$ or below before increasing loading on the foundation.

Ladd (1991) also indicated that soft foundations may experience long-term lateral displacements several times larger than what it may be measured at the end of

construction, and although the mechanisms causing this phenomenon are unclear. Ladd's opinion is that a causal factor of the continued shear distortions is "undrained" creep.

The relationships presented in Figure 2 are an attempt to show the relationship between the horizontal displacement and the settlement for an over-consolidated foundation based on the Palavas site reported in Tavenas et al. (1979) and presented in Ladd (1991). Case A exhibits a partially drained (DR=0.2) and undrained behavior (DR= 0.8) during fill placement, followed by consolidation having a deformation ratio (DR) of 0.15. Case B has an identical loading history as Case A, but the vertical drains provide significant drainage during fill placement (much larger settlement, slightly smaller lateral displacement at the end of construction). More rapid consolidation also reduces DR after loading due to smaller effects of "undrained" creep.
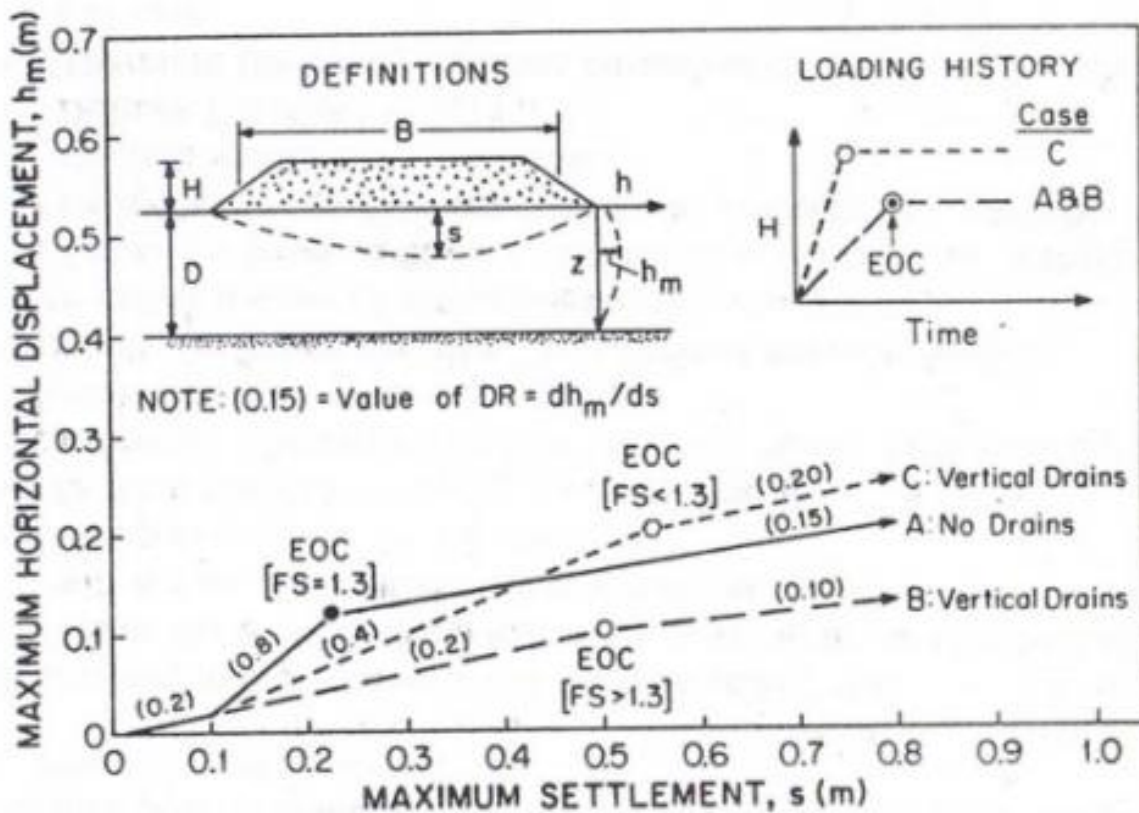

Figure 2. Schematic Relationship Between Maximum Horizontal Displacement and Maximum Settlement for Embankment Construction [adapted after Ladd. (1991) *Stability Evaluation During Staged Construction*]

In his 1991 Terzaghi Lecture, Ladd emphasized that significant variations from the schematic results presented in Figure 2 should be expected because the figure is based on limited specific field information for simple loading geometries, and the processes governing combined consolidation and creep behavior are not well understood, particularly with foundations having large zones of contained plastic flow. However, plots like Figure 2 are useful in monitoring the behavior of soft soil foundations.

Thus, interpretation of field data to warn of foundation instability requires considerable experience and judgement and the use of different plots depending upon the problem. Besides maintaining detailed records of time versus fill height (H), settlement (s) and horizontal displacement (h_m), Ladd (1991) suggested creating the following plots for monitoring foundation stability.

1. Periodic plotting of horizontal displacement h_d versus depth Z to locate weak zones and to locate the maximum horizontal displacement value (h_m)

2. h_m and s with H (fill height), with h_m generally providing clearer evidence of potential problems

3. h_m versus s to help detect partially drained versus undrained response and for comparison with prior behavior

4. During periods at constant load, evaluation of changes in dh_m/ds and dh_m/dt as a function of H and time. dh_m/dt should gradually decrease with time if controlled by consolidation. An increase in rate may imply excessive undrained shear deformation and impending failure.

Controlled rates of loading enable soil strengthening via consolidation to increase the stability of dams, embankments, landfills, tailings, and ash storage dams founded on or containing soft soil layers.(Ladd 1991)

When using the observational method to monitor the performance of facilities, at some point one must decide whether a facility is exhibiting levels of behavior that bring concern as to a potential impending failure of the facility. Hunter and Fell (2003) suggest that the ideal indicator of impending failure is one that consistently *"shows a significant change in response close to the failure."* However, to develop a practical methodology it must be determined how close to the failure the facility can be before intervening actions should be taken to prevent significant consequences. The engineering profession advocates for establishing threshold levels for the measurements being taken at the site in real time. One suggestion is to establish threshold and action levels for deformation parameters, based on understanding the stress-strain behavior of the foundation materials during laboratory tests.

Stress -Strain Behavior in Triaxial Compression Tests

In an effort to understand the stress-strain behavior of soils in a triaxial compression test, Lambe and Whitman, (1969), suggested to define three phases of the process of deformation of the soil:

1. The initial phase applies when the deformations are very small. In general, this phase advances up to vertical deformations of approximately 0.25%. During this phase, the sample will undergo a slight reduction in volume, as would be expected

with the increase of compressive stresses. In this phase, the particles re-adjust into a denser mass.

2. The intermediate phase begins when the sample compresses, and includes the maximum shear strength, and the gradual reduction on strength following the maximum. In general, this phase advances from approximately a vertical strain of 0.25% up to the value of the strain corresponding to the minimum value of shear strength.

3. The final phase is achieved when the shear resistance is constant even as the deformation continues. This phase is referred as final, ultimate, or residual strength. During the final phase of the test, the friction between the particles has diminished to the extent that deformation progresses without associated volumetric change.

The ratio of lateral and vertical deformations in a triaxial test with vertical loading indicate deformation ratios during the different phases of the test. During the initial phase of deformation, the deformation ratio is approximately constant, while the reorganization of the particles takes place. Values of the deformation ratio during this phase can be up to 0.2. When the deformations become large implying a failure, the deformation ratio would take values higher than 0.5. Results of a triaxial compression test are presented in Figure 3.
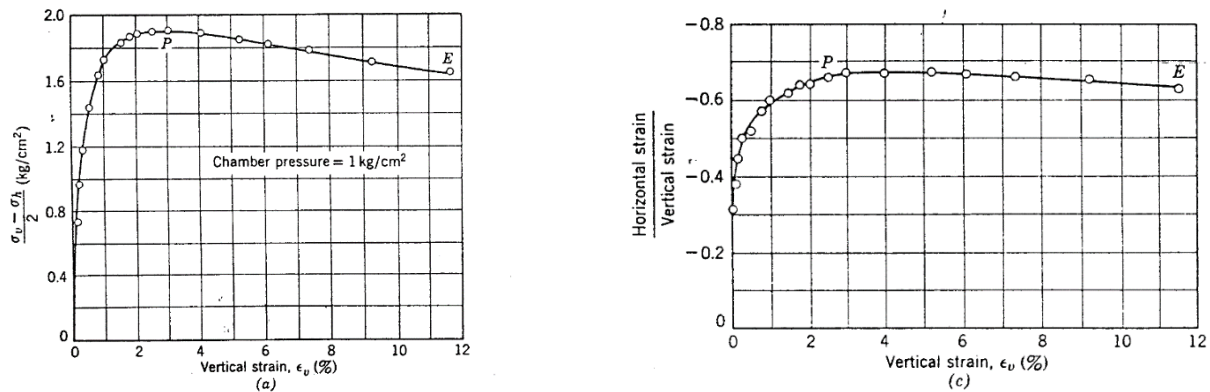

Figure 3. Results of a triaxial compression test on a well-graded calcareous sand. [adapted from Lambe and Whitman, Soil Mechanics, Figure 10.13(1969)]

III - STRESS-STRAIN BEHAVIOR OF CCRS

Triaxial Tests

A consolidated undrained triaxial (CIU) test was performed on a tube sample of an identified low strength layer of gypsum from a boring at a CCR site. The specimen was isotopically consolidated to 1.6 times the estimated in situ vertical effective stress. The measured friction angle at maximum obliquity was 30 degrees. Results of the test are included in Figure 4. Figure 5 is a plot of strain ratio versus axial strain for this test.

The CIU test was used to evaluate the horizontal strain/vertical strain ($\varepsilon_h/\varepsilon_v$) ratio from the CIU tests and to set threshold and action levels for the displacement ratios (DR) at the CCR facility. In monitoring the performance of CCR deposits, values of adjacent extensometers and inclinometers can be used to evaluate movement in the materials by calculating displacement ratios at elevations where movement is observed. The displacement ratio is defined as the cumulative horizontal deformation observed in the layer divided by the cumulative vertical settlement in the layer (D_H/D_V). Higher displacement ratios could be associated with the potential for shear induced lateral spreading, or undrained creep, as the friction between the particles has diminished to the extent that deformation progresses without associated volumetric change.

CIU tests on CCR materials often exhibit compressive behavior followed by dilative behavior before reaching the ultimate strength. The point where the contractive behavior transforms to dilative behavior is called the phase transformation point. At this point the average effective stress p' from the test is the minimum. In the CIU test presented here, the phase transformation occurs at an axial strain of 1.3% which corresponds to a $\varepsilon_h/\varepsilon_v$ ratio of around 0.54 as shown on Figures 4 and 5. Lambe and Whitman (1969) describe that when the deformations become large implying a failure, the strain ratio would take values higher than 0.5. Figure 5 exhibits inflection points at $\varepsilon_h/\varepsilon_v$ ratios of 0.18 and 0.54 which further illustrates changes in behavior of the material at these points.

SAMPLE INFORMATION

Boring: GEI-K2 Sample: U-02 Depth (ft): 23.8 ft Test: R'1
Type: 2.8-inch diameter Shelby tube sample
Description: Gypsum

SPECIMEN INFORMATION (after saturation)

Height: 5.948 in   Dia.: 2.893 in   Area.: 6.615 sq. in
Water Content: 30.4%   Dry Unit Weight: 85.8 pcf

TEST SUMMARY (end of test)

Effective Confining Stress: 2.44 ksf vertical, 2.44 ksf horiz.
Water Content: 29.1 %   Dry Unit Weight: 87.3 pcf
B Coefficient: 0.96   Strain Rate: 0.016 %/min
Peak Shear Stress: 1.04 ksf   @ 14.4 % Strain
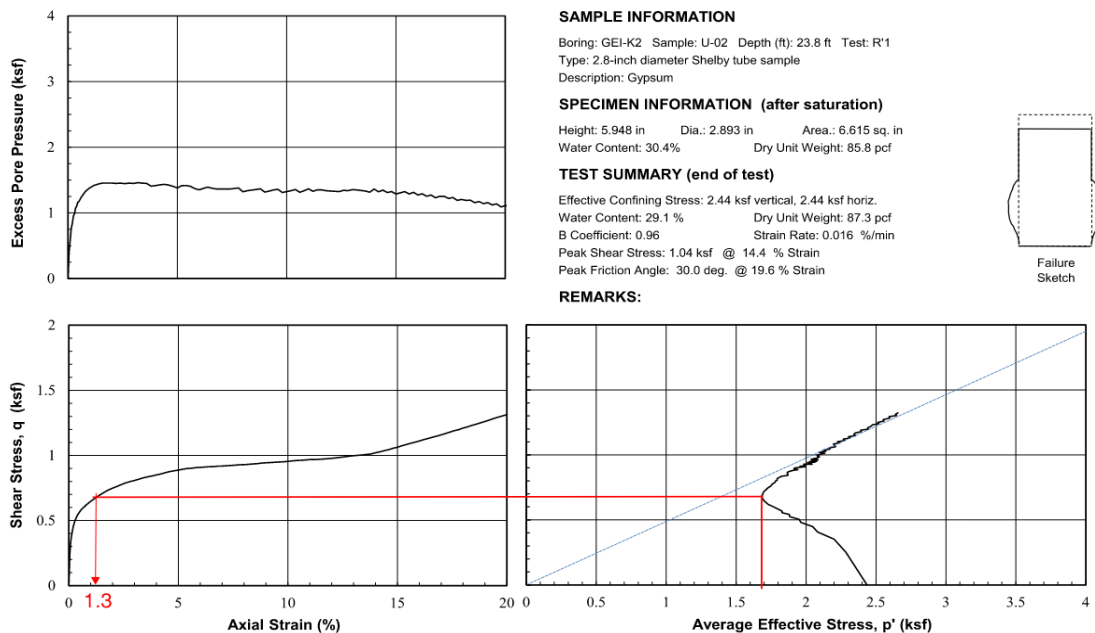Peak Friction Angle: 30.0 deg. @ 19.6 % Strain

REMARKS:

Figure 4. Results of a triaxial compression test on CCR materials

As described by Lambe and Whitman (1969), the initial stage, which is when straining is very small, extends to a strain of about 0.25%. During this initial phase of deformation, the values of the ratio are approximately constant while the reorganization of the particles is taking place. In the CIU test, the axial strain of around 0.25% corresponds to a $\varepsilon_h/\varepsilon_v$ ratio of 0.18 as shown on Figure 5.
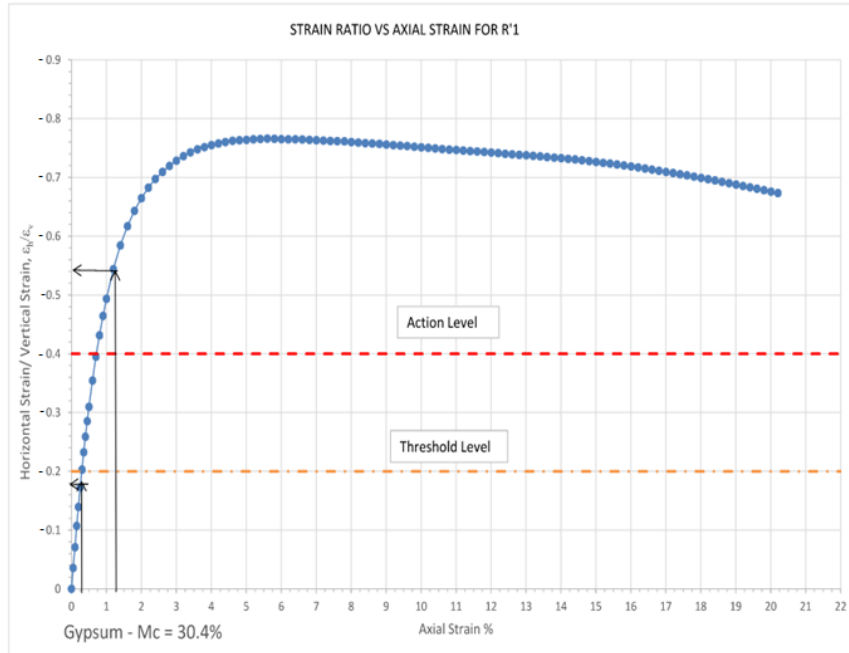
Figure 5. Values of the strain ratio based on results of a triaxial compression test on CCR materials

Direct Simple Shear Tests

Four direct Simple Shear Tests (DSS) were performed on tube samples of low strength gypsum from the same site as the CU' test above. The specimens were isotopically consolidated to 1 to 2 the estimated in situ vertical effective stress. In general, tests results exhibit contractive behavior of the material, with an initial peak strength and then a reduction to a residual strength as the strain continues. Figure 6 depicts typical results of DSS on CCR materials. Figure 7 shows a summary of results of the four tests.
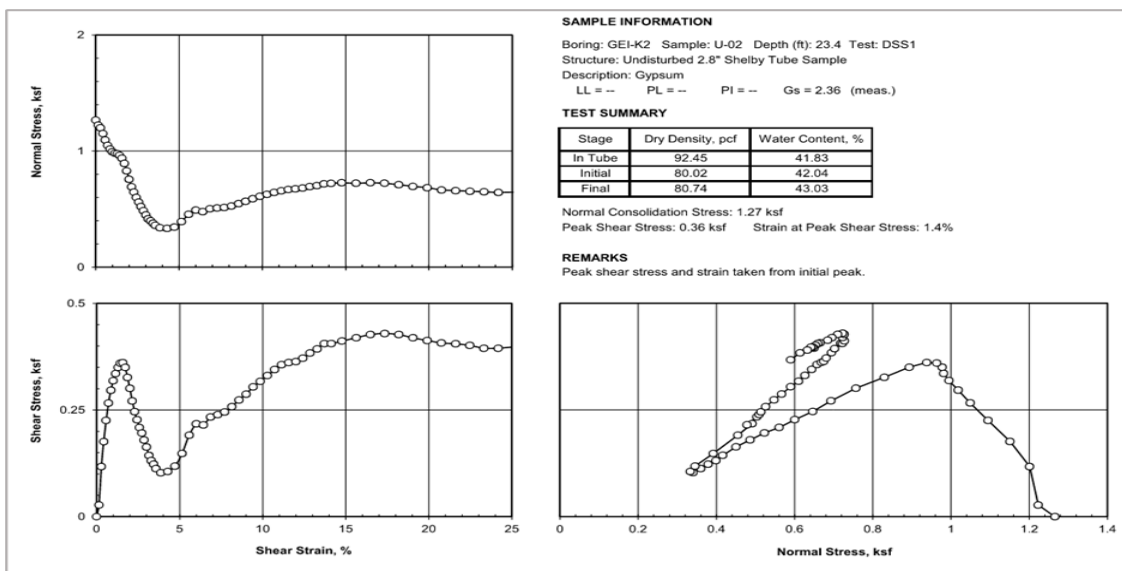
Figure 6. Typical results of a Direct Simple Shear test on CCR materials
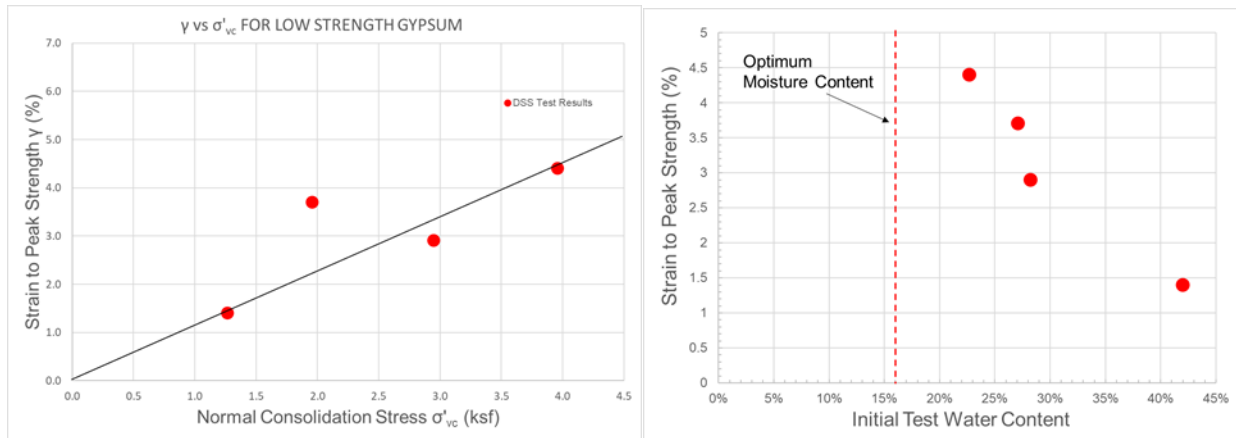
Figure 7. Summary of results from Direct Simple Shear tests on CCR materials

Furthermore, Figure 7 illustrates the relationship between moisture content of the material and the magnitude of shear strain necessary to reach peak shear strength. Centrifuge tests performed on fly-ash at a dense state and at a moisture content of appx. 4% above the optimum moisture content of the material revealed that upon opening of the gates of the sample holder, the fly ash exhibited a slope instability failure. Whereas a test performed on the same fly- ash at a loose state and at moisture content appx. above 16% of the optimum moisture content of the material revealed that upon opening of the gates of the same sample holder, the fly ash exhibited a sudden flow failure. EPRI (2021)

Hunter and Fell (2003) suggest that the ideal indicator of impending failure is one that consistently *"shows a significant change in response close to the failure."* Based on the above discussion, settlement and inclinometer data were used to monitor the behavior of CCR disposal facilities affected by changes in loading conditions following their hydraulic depositions. Typical cross-sections of the different facilities were monitored to evaluate the deformation response to those changing conditions.

IV – ILLUSTRATIVE CASES

The applicability of using deformations to monitor short- and long-term performance of CCR facilities is presented as it may apply to two common scenarios of construction over soft, saturated CCR deposits.

Case 1 – Construction of a fill over hydraulically deposited Fly Ash

A facility undertook the construction of lateral and vertical expansion of an existing Residual Waste Landfill. The new expansion was designed to be completed in several phases. The general site plan for one of the phases required the construction of a 65-foot-high embankment to provide containment to the proposed landfill and accommodate its leachate collection appurtenances. The fill extended over a fly ash impoundment approximately 7 acres in size near its decanting structure and therefore where the finest fly ash particles had concentrated over the storage life of the impoundment. The monitoring period covered construction of the stabilization of the fly

ash surface and the construction of the proposed fill. The fill location with respect to the fly ash impoundment is shown on Figures 8 and 9.

Figure 8. Project Area

Construction of the fill of the proposed landfill expansion, Figure 9, was planned to achieve final grade elevations ranging from approximately El. 686 towards the existing dam to approximately El. 687 away from the former impoundment, taking the northern section of the fill near the final elevation of the proposed high bench to the toe well within the deposited fly ash.
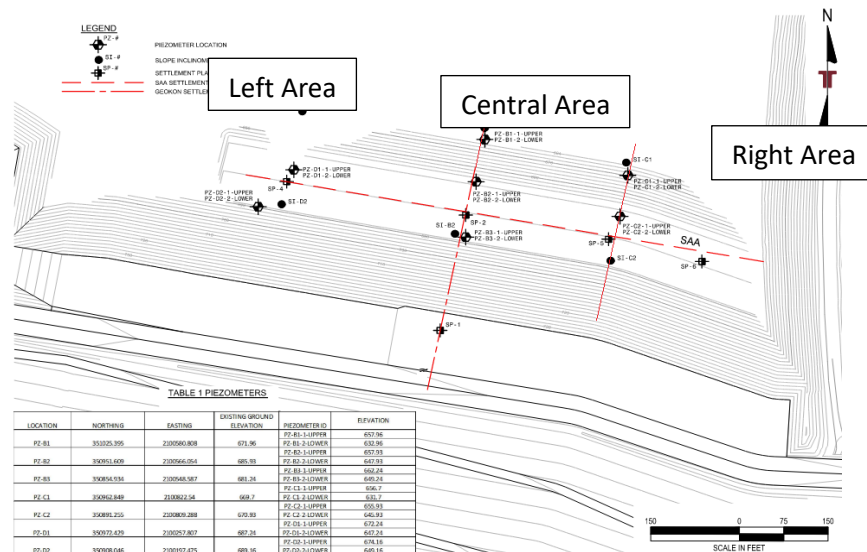
Figure 9. Landfill expansion final grades and Instrumentation location.
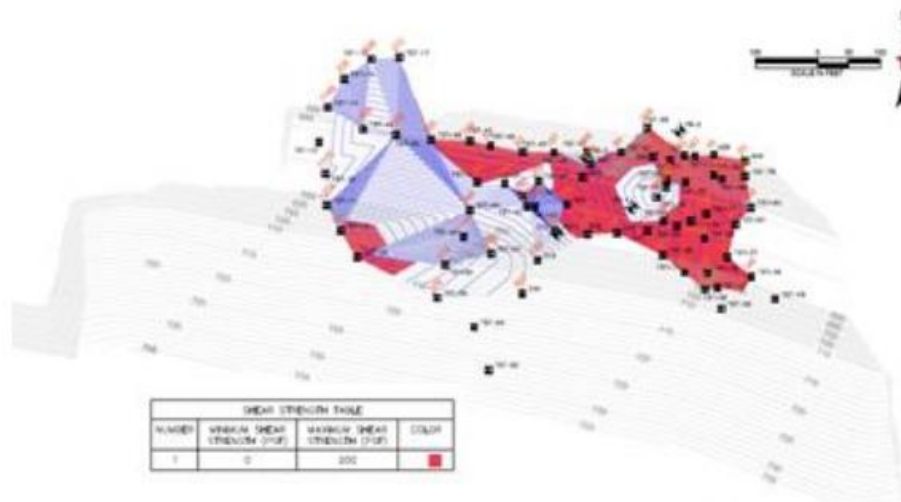
Figure 10. Subgrade strength under fill areas.

The proposed fill construction was subdivided into different areas based on the relative strength of fly ash subgrade as illustrated in Figure 10. The central and left placement areas revealed a relatively stronger subgrade (blue contours) than the right area, which revealed a subgrade strength of less than 200 psf. (red contours)

The Contractor's construction plan called for all the subgrade within these placement areas to be reinforced by using geogrids lying upon the exposed fly ash surface. A bridge layer of bottom ash was placed on the geogrid followed by subsequent lifts of sand as the structural fill. The bottom ash layer also served as a capillary break.

Performance of the fly ash deposit was initially planned to be assessed by using several pore-pressure monitoring devices only. Data collection was made at a high frequency as the contractor's consultant desired "real time" feedback. As the structural fill placement advanced, pore pressure monitoring provided the expected feedback: high excess pore-pressure buildup followed by quick dissipations. In addition, however, the placement of fill on the fly ash subgrade also led to the fly ash foundation experiencing vertical as well as horizontal deformation, which at the time were not being monitored.

Anecdotal evidence revealed that as the bridge layer advanced over the fly ash subgrades, "mud waves," or lateral deformations, were observed. On October 21, 2015, piezometers recorded a high excess pore-pressure event, which coincided with a subgrade failure. Following the failure of the bottom ash bridge/ capillarity break layer, the foundation was improved by driving a large rock layer into the fly ash foundation to create a stable soil matrix within the footprint of the embankment in the area near the dam before the geogrids were laid down again. The improvement technique used was deemed successful as it allowed the continuation of the fill placement while experiencing similar high excess pore-pressure events without failure.

Following this construction incident, it was concluded that monitoring the construction of the proposed fill with only pore pressure observations would not provide sufficient

advance warning of an impending failure. Thus, it was decided that while it was prudent to add additional pore-pressure monitors, a series of slope indicators and associated settlement plates would also be installed to monitor both lateral and vertical deformations. Figure 9 depicts the locations of the additional deformation monitors.

Pore Pressure

The placement of fill on the fly ash subgrade led to the fly ash experiencing a buildup of excess pore pressure and subsequent dissipation of it as the fly ash particles took on the load, as illustrated in Figure 11. In general, the behavior of the pore pressure is affected by the rate of load application, the permeability of the fly ash mass, and the position of the water table, which in turn is affected by the precipitation and runoff into the area. Pore pressure was monitored using seven piezometer locations, each location containing two vibrating wire sensors located at two different depths within the saturated fly ash.
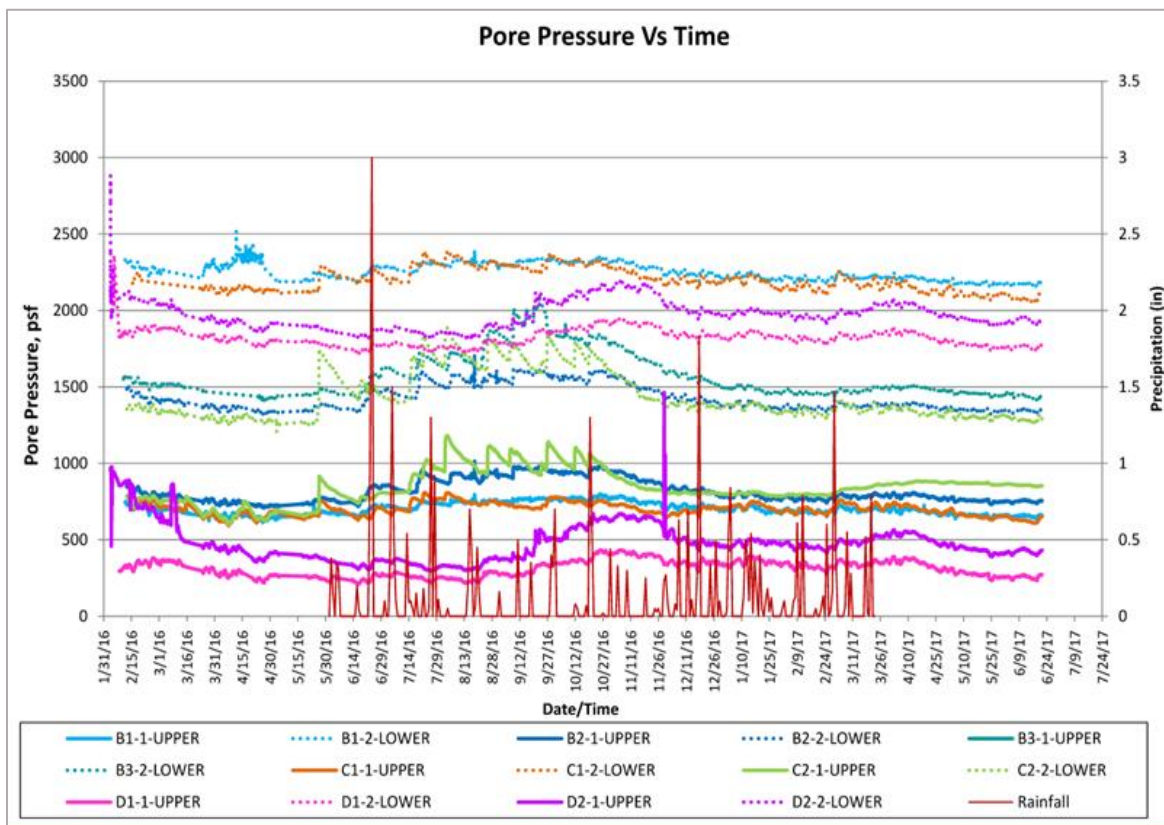
Figure 11. Variation of Pore Pressure with Time, including precipitation data.

In general, the highest excess pore pressure values recorded in the piezometers during the placement of structural fill embankment were lower than the values recorded during the placement of the capillary break/bridge layer over the fly ash subgrade prior to the instability being experienced near the dam, and lower than the values recorded within the same area following the subgrade improvement work. Variation of the non-

12

dimensional parameter Ru with time are shown below in Figure 12, where Ru = $\Delta\mu/\Delta\sigma_v$ with $\Delta\mu$ = change on pore pressure, and $\Delta\sigma_v$ = change on applied stress.
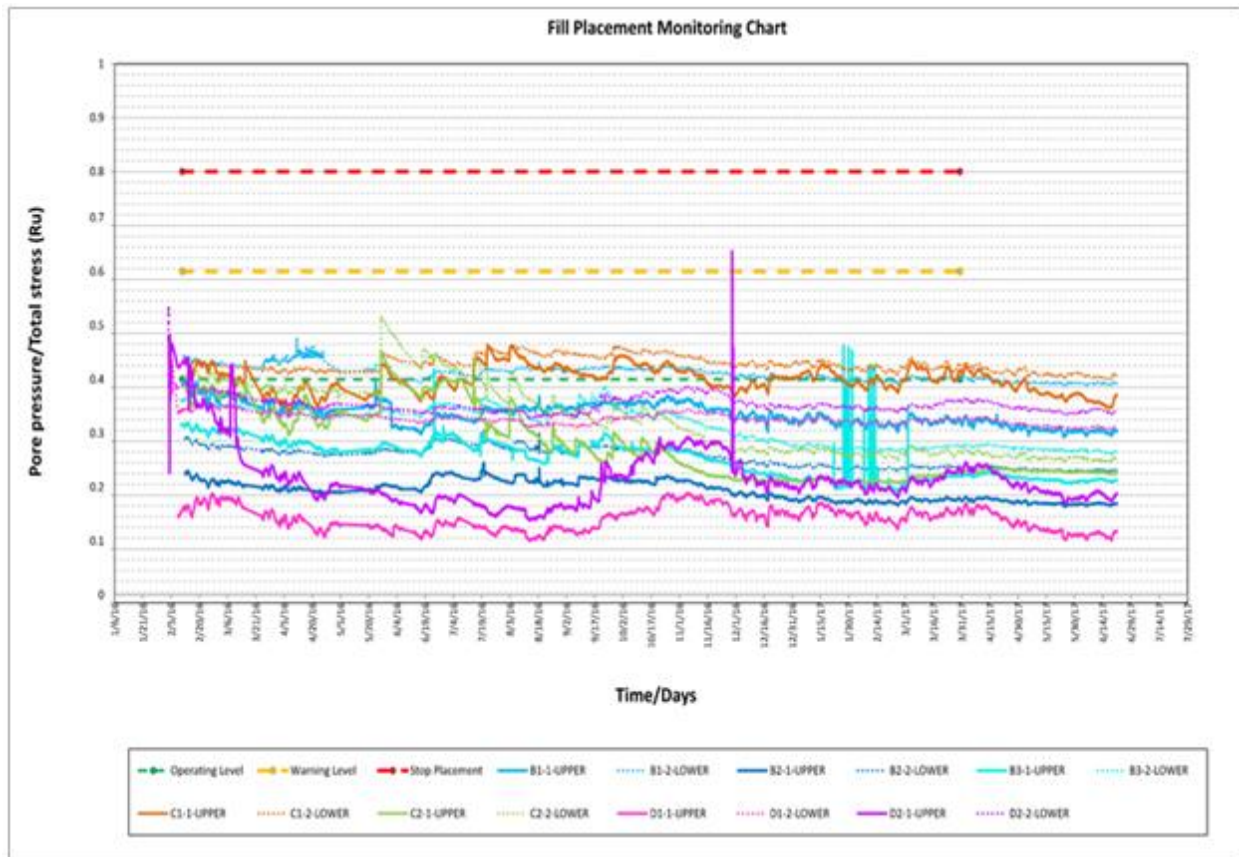
Figure 12. Variation of Ru with Time.

Ru thresholds for this project were established based on the work of Tavenas and Leroueil (1980) that presented a compilation of pore pressure observations available in the literature for the early stages of embankment construction. In their review, Tavenas and Leroueil (1980) determined that pore pressure response on initial loading was variable with Ru values ranging from 0.1 to 0.8, and the response after reaching the maximum threshold state was ≈ 1.0. They also concluded that a value of Ru "*of the order of 0.4 is significantly below the theoretical value corresponding to an undrained behavior.*" On this basis, action thresholds were set for this construction at 0.4 and 0.6 as warning values leading to an increase in the frequency of recording and reviewing of the data. A value of 0.8 would lead to stopping all construction activities within the compromised loading area.

As shown on Figures 11 and 12, all piezometers recorded consistent trends in their behavior. None of the values determined indicate that the Ru levels of concern were reached during the period of construction to trigger a change of monitoring frequency or the stopping of construction.

Vertical Displacement

The vertical deformation of the fly ash deposit was monitored using six settlement plates. Settlement plates were set at elevations near the fly ash subgrade but on top of the bridge layer. Settlement plates SP- 1 (El. 682.5), SP-2 (El. 684.0); SP-3 (El. 672.0) were located up the slope above the bench, at the bench, and at the toe along the central cross section of the loaded area, respectively. Settlement plate SP-4 (El. 687.6) was located at the bench of the slope left of the central cross section of the loaded area. Settlement plates SP-5 (El. 671.0) and SP-6 (El. 671.5) where located on the bench of the slope right of the central cross section upstream of the dam. Overall settlement plate movements are shown on Figure 13.
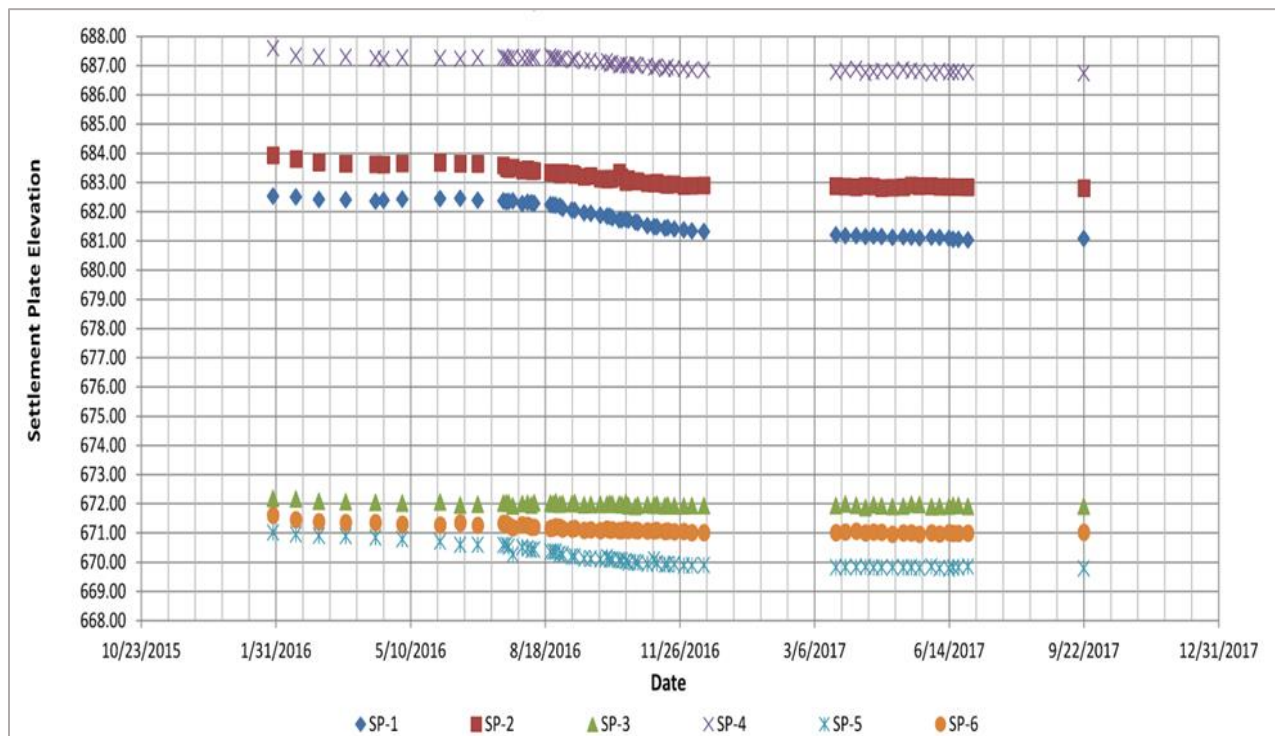
Figure 13. Overall movement of Settlement Plates over the monitoring Period.

Horizontal Displacement

The horizontal deformation of the subgrade due to loading was monitored using six inclinometers located along the cross sections shown on Figure 10. SI- B1 (El. 671.8) at the toe and SI-B2 (El. 687.5) at the bench were located on the same alignment as SP-1, SP-2 and SP-3, along the central cross section of the slope. SI-C1 (El. 669.4) at the toe and SI-C2 (El. 686.07) at the bench slope are right of the central cross section, upstream of the dam. SI-D1 (El. 678.2) at the toe and SI-D2 (El. 687.4) at the bench are left of the central cross section of the loaded area. To determine if the fly ash subgrade exhibited a significant change in response to the loading, which may indicate a potential for failure, maximum settlement and lateral displacement were reviewed for the selected cross-sections.

CENTRAL CROSS-SECTION

The central cross section geometry and instrumentation are shown on Figure 14. SP-1 was located to capture the settlement of the subgrade near the maximum loading condition. Settlement with time and settlement in response to fill placement are shown in Figure 15.
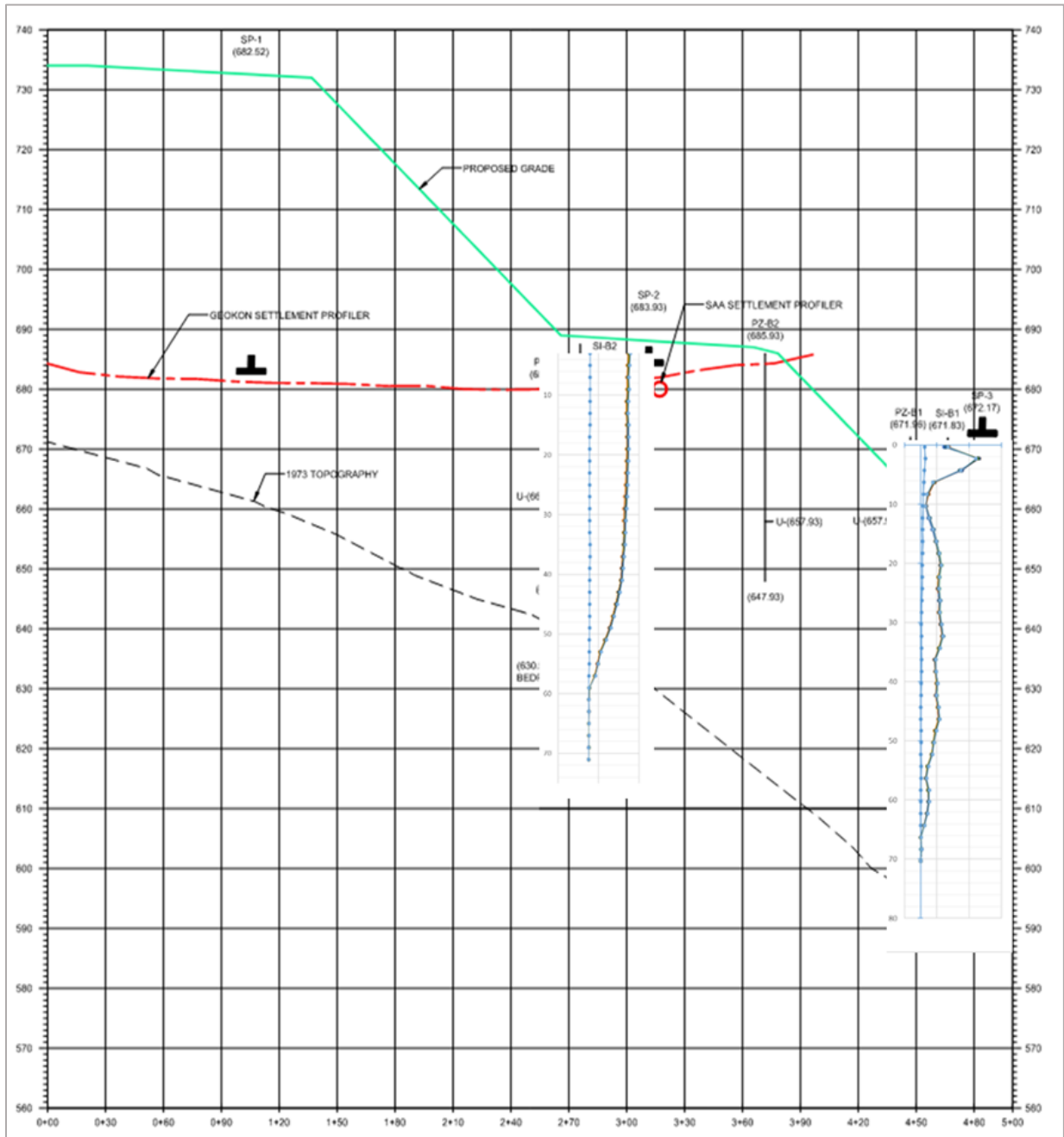
Figure 14. Central Cross Section of fill, depicting the location of settlement plates and inclinometer movements.
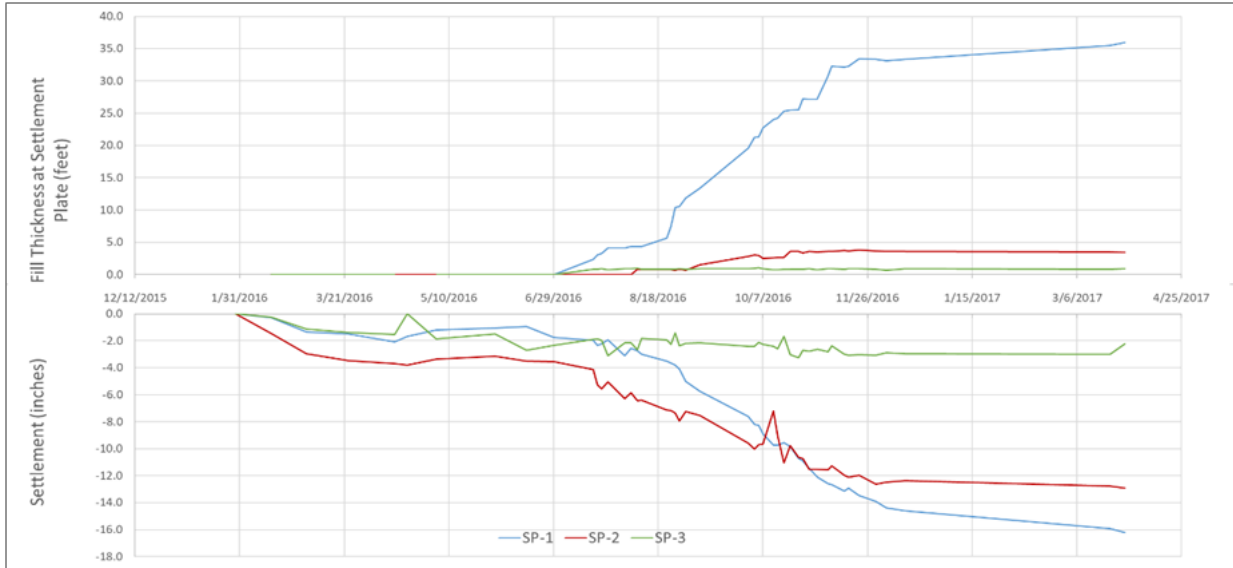
Figure 15. Fill thickness and Settlement Plate movement with time.

Settlement along the cross-section ranged from nearly 4 inches at the toe of the loaded area to nearly 18 inches at the location of SP-1, near the maximum load. Based on the shape of the settlement versus time plot, Figure 15, It should be noted that by the time of the final fill thickness was placed over SP-1, at least 90% of the consolidation settlement of the fly ash subgrade had occurred
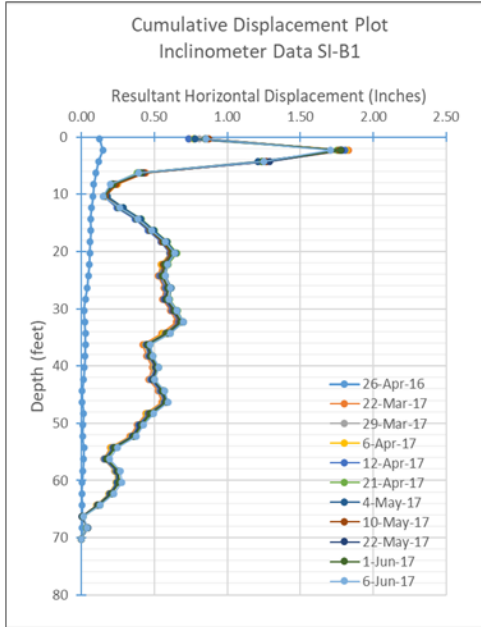
Figure 16. Horizontal Displacement with depth at **toe** of the embankment within this placement area.
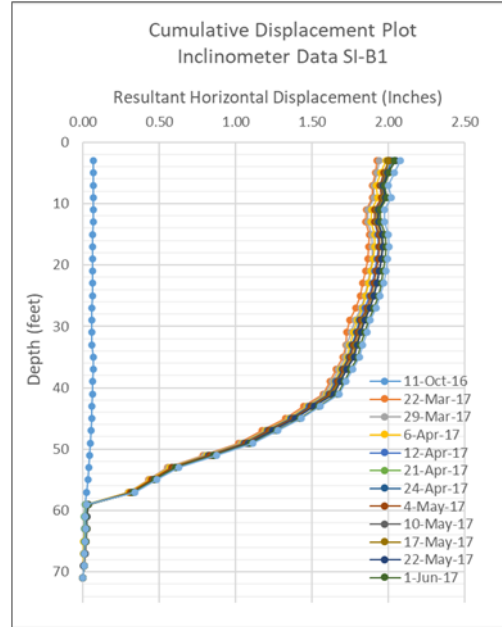
Figure 17. Horizontal Displacement with depth at the **bench** of the embankment within this placement area.

Horizontal displacements of the fly-ash deposit were monitored with slope indicators B1 and B2, at two locations of interest, and the associated vertical displacement was

recorded with settlement plates SP1 and SP2. Horizontal displacements are shown in Figures 16 and 17, and the variation of Horizontal displacement with fill height (load) is shown on Figure 18, The relationship between horizontal and vertical displacements is shown in 19.

At the toe of the slope, inclinometer SI-B1 recorded a maximum horizontal deformation of just above 1.3 inches near the surface of the fly ash reflecting the horizontal movement of the "mud wave" as the subgrade was loaded. Horizontal deformations of approximately 0.6 inch were recorded within the fly ash deposit between approximate depths of 20 to 45 feet below the ground surface. At the bench of the slope, inclinometer SI-B2 recorded horizontal deformations of about 2.2 to 1.8 inches between depths of 10 and 40 feet below the ground surface.
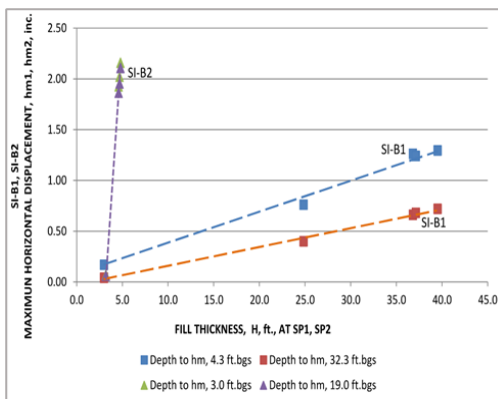
Figure 18. Variation of the Maximum Horizontal Displacement, h_m, with fill thickness above Settlement Plates in central area.
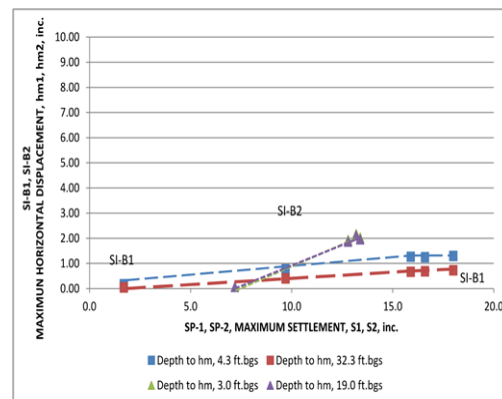
Figure 19. Relation between the Maximum Horizontal Displacement, h_m, and Maximum Settlement, s, in central area.
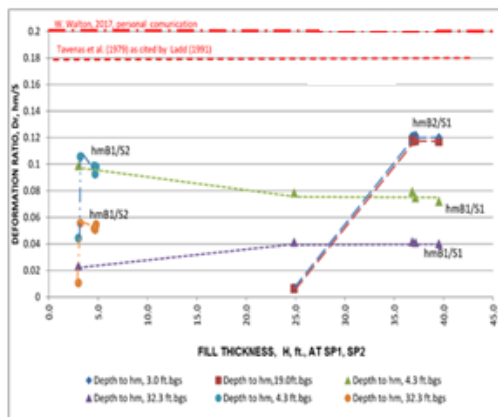
Figure 20. Deformation Ratio versus time within the central area.
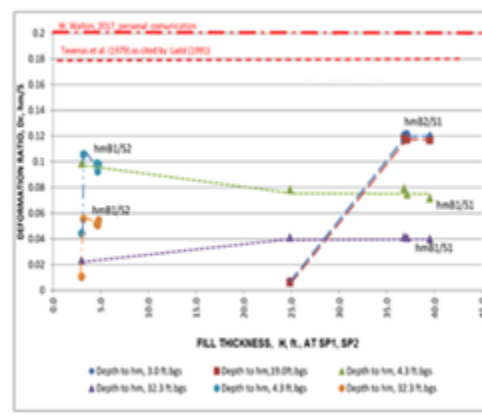
Figure 21. Deformation Ratio versus fill thickness (load) at the location of the settlement plates in central area.

By the time the last set of readings, within the scope of this monitoring effort was performed, approximately 3 months after the fill had reach its final elevation over SP-1, little additional settlement had taken place. Based on field observations, it is concluded

that during the construction of the fill the deformation did not exceed the magnitude expected during consolidation, based on the values of the ratio being approximately constant. Deformation ratios versus time and fill thickness are shown in Figures 20 and 21.
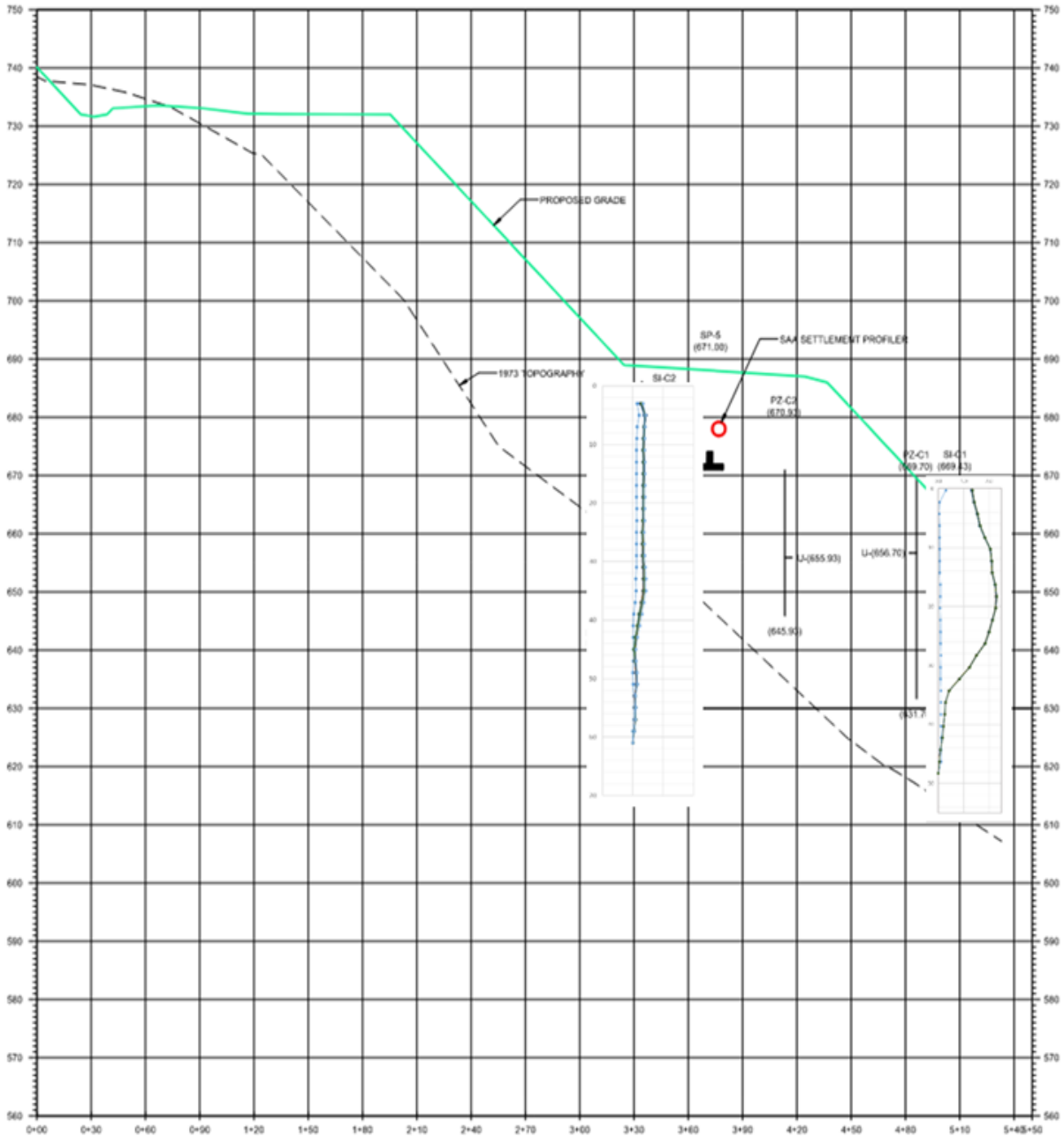
RIGHT CROSS-SECTION

Figure 22. Section of placement area right of center, depicting the location of settlement plates and inclinometer movements.

Figure 23. Fill Thickness and Settlement Plate movement with time.

Settlement plate SP-5 was located near the fly ash subgrade under the bench of the fill within the right area of the fill near the dam, SP-6 was located near the fly ash subgrade under the bench of the fill, but over the upstream slope of the existing dam. The location of these settlement plates in relation to the cross section of the fill slope, to the thickness of the fly ash deposit, and to other instrumentation is shown on Figure 22.

Settlement within this fill area ranged from nearly 8 inches at SP-6 to over 14 inches at the location of SP-5. Settlement plate movement with time and in response to fill thickness are shown in Figure 23.
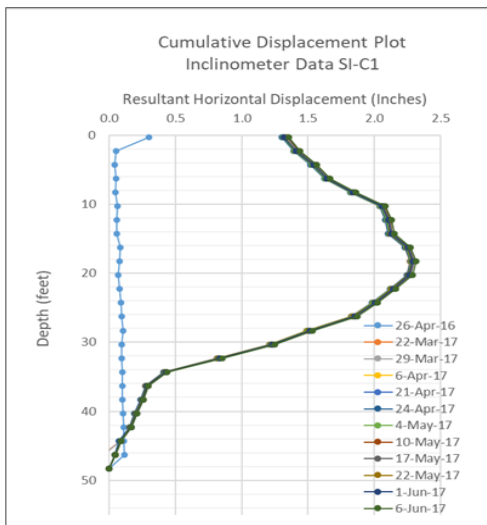
Figure 24. Horizontal Displacement with depth at **toe** of the embankment within the right area.
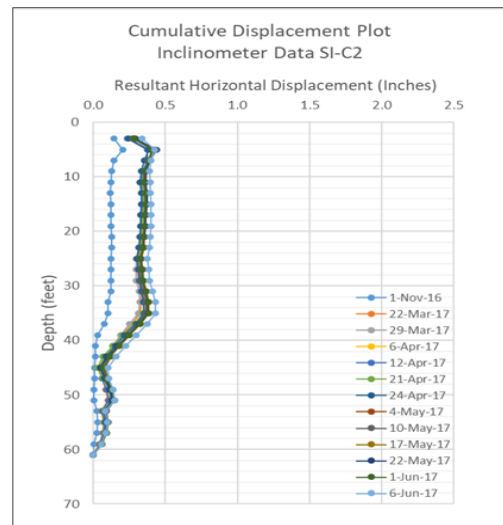
Figure 25. Horizontal Displacement with depth at the **bench** of the embankment in the right placement area.

In inclinometer SI-C1, a maximum horizontal deformation of about 2.3 inches was recorded within the fly ash deposit at a depth of approximately 20 feet below the ground surface at the toe of the fill near the boundary of the subgrade improvement area, as shown on Figure 24. Horizontal deformations were recorded at two depths of interest below the fill's bench, in inclinometer SI-C2.A maximum horizontal deformation of about 0.43 inches was recorded at a depth of 6 feet below the ground surface and a horizontal deformation of approximately 0.48 inches was recorded at a depth of 35 feet below the ground surface, as shown on Figure 25.
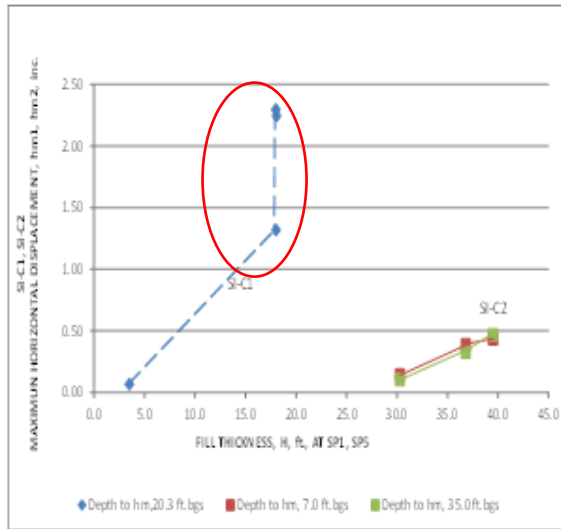
Figure 26. Variation of the Maximum Horizontal Displacement, h_m, with fill thickness above Settlement Plates in the right placement area.
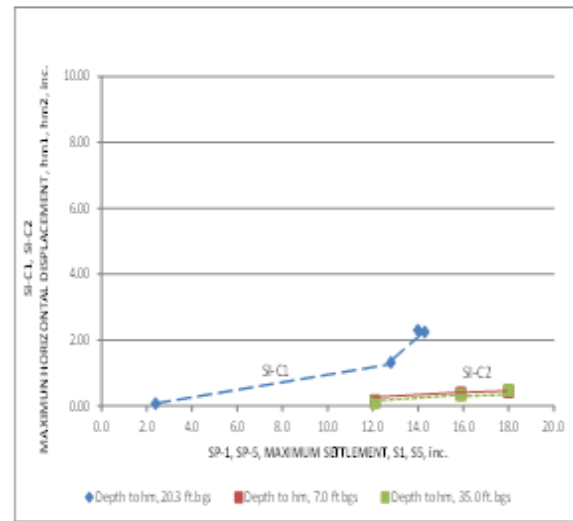

Figure 27. Relation between the Maximum Horizontal Displacement, h_m, and Maximum Settlement, s, in the right placement area.
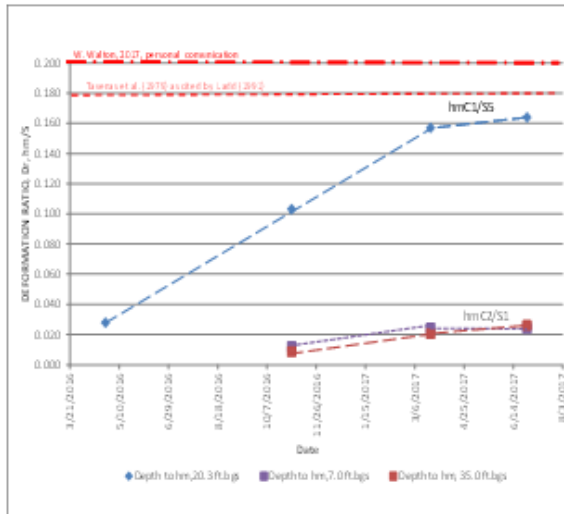

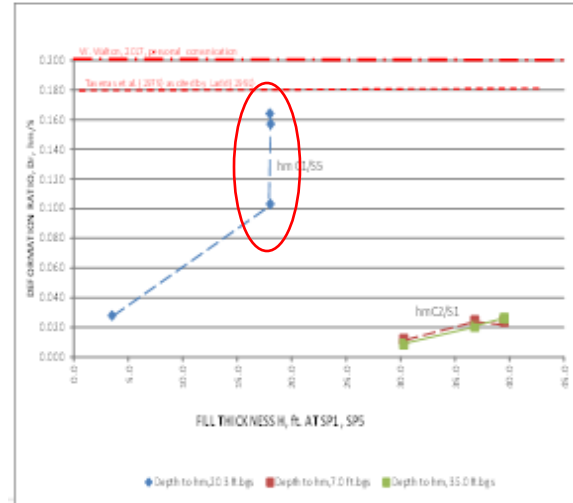Figure 28. Deformation Ratio versus time in the right placement area.

Figure 29. Deformation Ratio versus fill thickness (load) at the location of the settlement in the right placement area.

Horizontal displacement versus time and fill thickness are shown in Figures 26 through 29. During the construction of the fill the deformation did not exceed the magnitude expected from the consolidation phase. The values of the ratio became approximately constant as the reorganization of the particles was taking place, as shown in Figure 28. However, as the height of the fill over SP5 reached its maximum elevation, the horizontal deformation observed in SI-C1 continued to increase indicating horizontal creep, as shown in Figure 26. While similar behavior is observed in the deformation ratio of SI-CI/ SP-5, in Figure 29, the magnitude of the ratio (less than 0.2) indicates that the movement is most likely associated with consolidation of the subgrade under the area improved to facilitate the placement of the bridge/capillary brake layer.

As depicted in Figure 23, by the time the final fill thickness was placed over SP-1 at least 90% of the consolidation settlement of the fly ash subgrade had occurred in this area of the subgrade. By the time the last set of readings within the scope of this monitoring effort was performed , approximately 3 months after the fill had reach its final elevation, a small additional settlement was recorded at SP-5, whereas no appreciable settlement was recorded at the location of SP-6.

Comparison of Field performance with Laboratory Test Results

During the design of the fill, consolidation tests on samples of the fly ash were conducted to estimate the magnitude of the settlement that could be experienced by the facility and its potential effects on permanent drainage features of the landfill expansion. To compare the field deformation behavior of the fly ash with the behavior of the fly ash observed in laboratory tests, a plot of the values of the constrained modulus, $M = \Delta\sigma'_v / \Delta\varepsilon_v$, where $\Delta\sigma'_v$ is the change in vertical effective stress and $\Delta\varepsilon_v$ is the change in vertical strain, was developed. The field values of M were back calculated by determining $\Delta\sigma'_v$ and $\Delta\varepsilon_v$, ($\Delta\varepsilon_v = s/h_{fa}$, where s is the settlement of the settlement plate and h_{fa} the thickness of the fly ash deposit), at the location of the settlement plate.
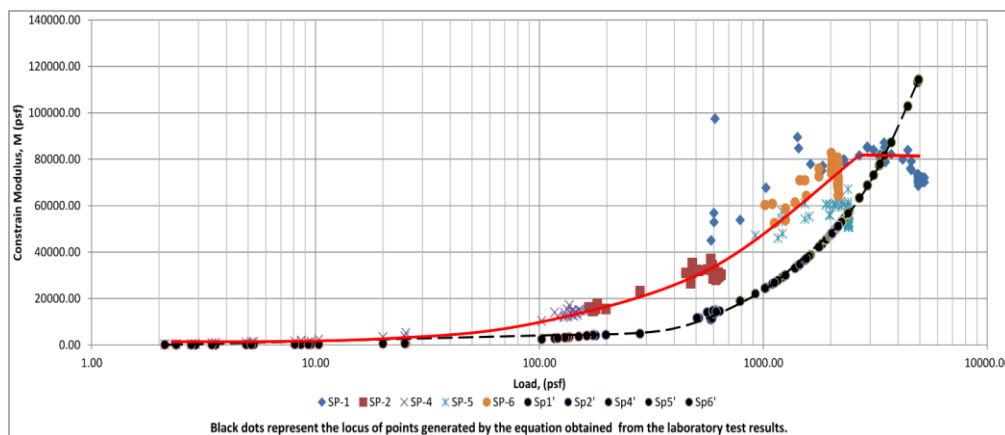

Figure 30, Comparison of values of M obtained in the laboratory and values of M back calculated based on actual vertical deformation observed during fill placement at the settlement plates.

It can be observed that the back calculated value of M (colored dots) was, in general, higher that the value determined in the laboratory for the same applied load, illustrating that the foundation material is stiffer, within the range of acting stresses, than anticipated. Thus, supporting the expectations that the drainage features of the facility would perform as intended in the design However, the field values seem to reach a limiting value, which at this site is approximately 80,000 psf. The drop on value of M, experienced at the tail of the data, may be attributed to the estimating methodology use to determine the actual load at the location of the plate, meaning additional fill was placed to compensate for settlement which was not accounted for. This leads to an underestimate of vertical stress and therefore an underestimate of constraint modulus.

Case 2 – Dry CCR Stack over Hydraulically Deposited CCR

A CCR facility consisting of two adjoining former sluiced gypsum and fly ash disposal ponds, West Pond and East Pond, is shown on Figure 33. The facility was opened in 1986 as sluiced gypsum storage. The ponds were originally constructed as one pond retained by a starter dam (perimeter dike) comprised of compacted clayey mine spoil to the south that ties into high ground to the east and west. A stilling pond was constructed within the perimeter dike, and gypsum/fly ash dikes were constructed to the north of the stilling pond. In 1996, the height of the perimeter dikes was raised using upstream dike construction methods. The raised dikes were constructed of co-mingled gypsum and fly ash. A divider dike was also constructed to separate the East and West Pond. Sluicing of co-mingled gypsum and fly ash continued until 2011 when the facility was converted to a dry stack. Dry stacking of co-mingled gypsum and fly ash continued at the ponds until 2019.

Figure 31. Project Area

The stack was generally constructed with 3H:1V slopes and 15-foot-wide benches in between sloped sections of the dike. The stack is comprised of gypsum up to approximately El. 484, and a mixture of gypsum and fly ash from El. 484 to the current stack maximum height at approximately El. 545. In 2017, the East Pond was partially closed. CCR material was removed from the East Pond and the side slopes of the east slope were flattened to approximately 5H:1V to 6H:1V. Surface water let downs were constructed to facilitate rainwater drainage off the stack. The piezometers located within the former East Pond showed that the water level in the stack dropped around 4 ft between 2018 and 2021.

History of Movements

In 2008, a surface slough with seepage of the southeast portion of the West Pond dike was noted. The area was reportedly wet and soft prior to the final failure. The area was repaired. In 2009, multiple wet areas in the perimeter dikes and standing water in most of the intermediate benches in both the East and West Pond were noted. Areas of sloughing and slumps along the perimeter of the East Pond were also observed. At the time, explorations were performed, and standpipe piezometers were installed to define the piezometric level and asses the stability of the stack.

Between 2009 and 2010, several repairs along the dikes of the East and West Ponds including slope armoring, flattening of slopes, ditching, and buttressing to improve static slope and seepage stability to acceptable factor of safety were performed. The most significant repairs were implemented on the north and south slopes of the East Pond. Because of the sloughing observed in 2009 on the south slope of the East Pond, a small toe buttress was installed to stabilize the slope along the north side of the stilling pond. However, movement continued after the buttress construction. Two borings were drilled from the top of the buttress to install slope inclinometers to determine the depth of the potential failure plane. After stability analyses were performed on the slope, a larger toe buttress approximately 55 feet wide that spanned the entire length (approximately 1,500 ft) of the south slope was built to successfully stabilize the slope along the stilling pond. In the field, the rock buttress was extended to the east slope of the West Pond, which was also showing signs of excessive movement.

Inclinometer data have shown that the south slope of the East Pond had an increase in rate of movement from the summer through fall of 2016. Based on anecdotical evidence, it was concluded that the movement was likely triggered by lowering of the water level in the Stilling Pond for spillway reconstruction from July through October of 2016. The east slope of the East Pond also exhibited movement within the gypsum/fly ash layer around the same period. At the time, it was concluded that this movement was likely a localized shallow movement that was the result of increased rainfall.

In 2017, unusual readings were reported for in-place inclinometers at the East and West Pond. To investigate possible progressive moment of the stack, or data errors in the instrumentation recordings, the data were reviewed and stability analyses were performed using the existing site conditions. This effort concluded that global stability factors of safety were adequate. However, Sections on the south slope of the ponds

were found to have marginal factors of safety associated with failure surfaces within weaker layers if the planned dewatering activity were to increase the acting effective stresses.

No significant changes in topography have occurred since 2017. Figures 32 and 33 depict representative cross-sections of the west and east ponds respectively. Closure of the facility is expected to start in 2022. The proposed closure conditions are expected to reduce loading within the stack making it more stable in the long term. The cross-sections in Figures 34 and 35 reflect the current topography, and proposed closure final geometry (red line). For ease of presentation, the sections have been labeled K-K at the West Pond and H-H at the East Pond.
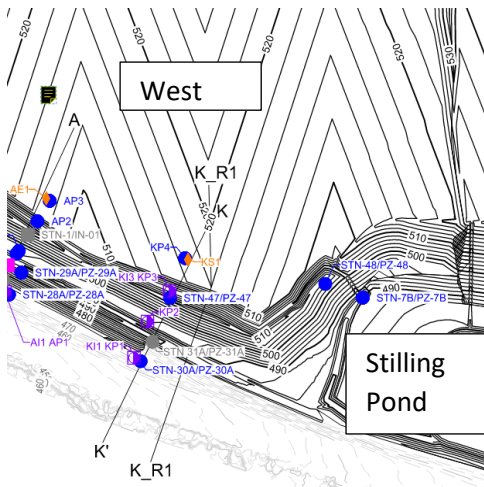
Figure 32: West Pond, Section K-K
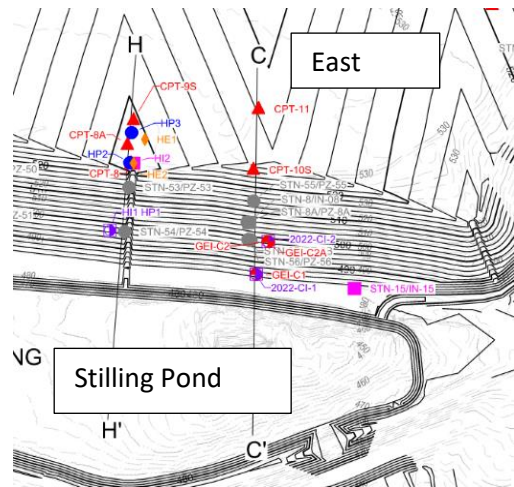
Figure 33: East Pond, Section H-H
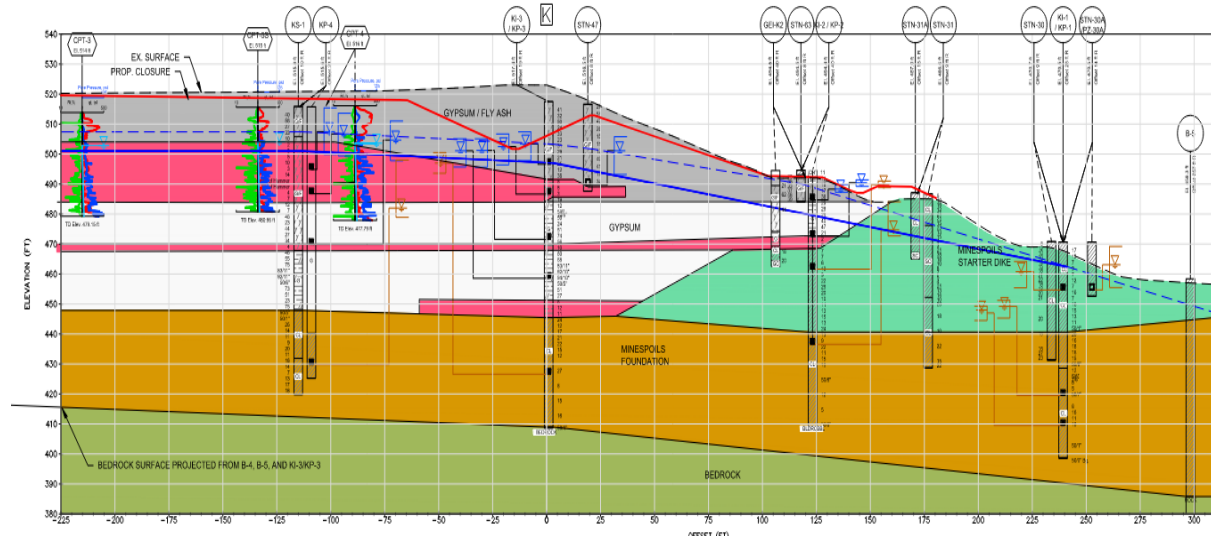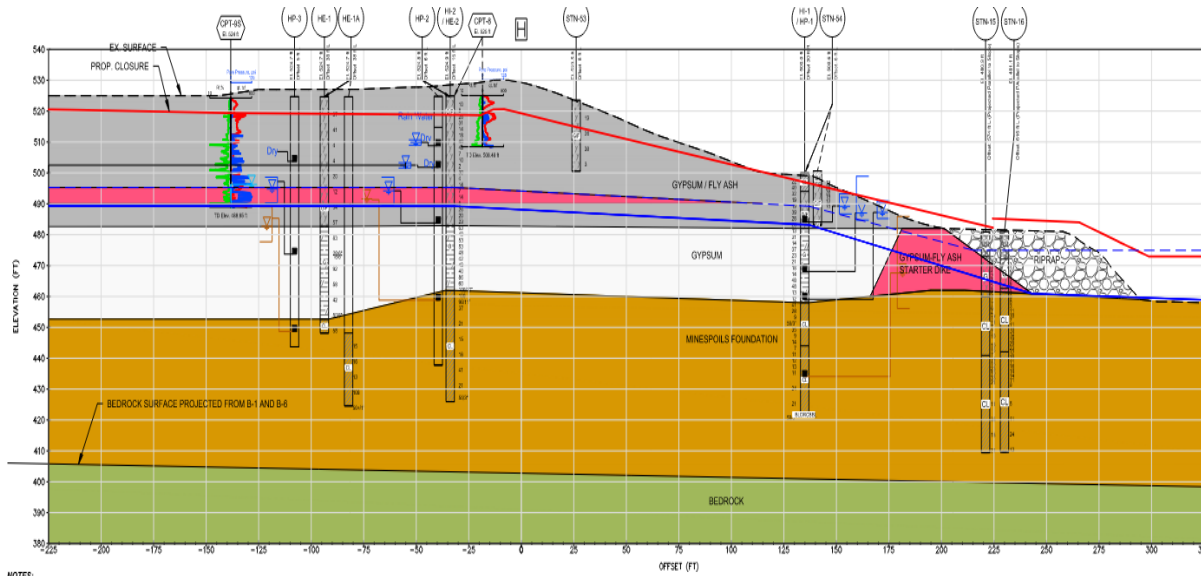

Figure 34. Section K-K

24

Figure 35. Section H-H

Layers within the Gypsum and Gypsum/Fly Ash that had low SPT-N (blow-count) values, when compared to the values in the surrounding material, were deemed to be zones of low strength. Figures 34 and 35 depict zones of lower-strength, soft or loose material. Individual SPT-N values below 14 blows per foot (bpf) were used as the criteria to identify layers susceptible to significant response to changes in effective stress.

Movement Evaluation

Six inclinometers were installed in 2010 because of the observed movements in 2009. In 2014, 12 additional inclinometers were installed. Throughout the years some inclinometers have been abandoned either because of site regrading or because excessive movement in the casing prevented the probe from advancing to take readings. There are seven active inclinometers at the CCR facility. Four magnetic extensometers and one Sondex settlement system were also installed in 2014.

The active instruments were used to evaluate movements at the stack and the associated loading mechanisms that could explain the movements. The height of the stack has not changed significantly since 2017. However, the water levels within the CCR stacks have fluctuated, as shown on Figures 36 and 37, and therefore effective vertical stresses acting on the weaker layers have also changed accordingly, causing a loading mechanism that has led to the displacements observed along the layers of interest.
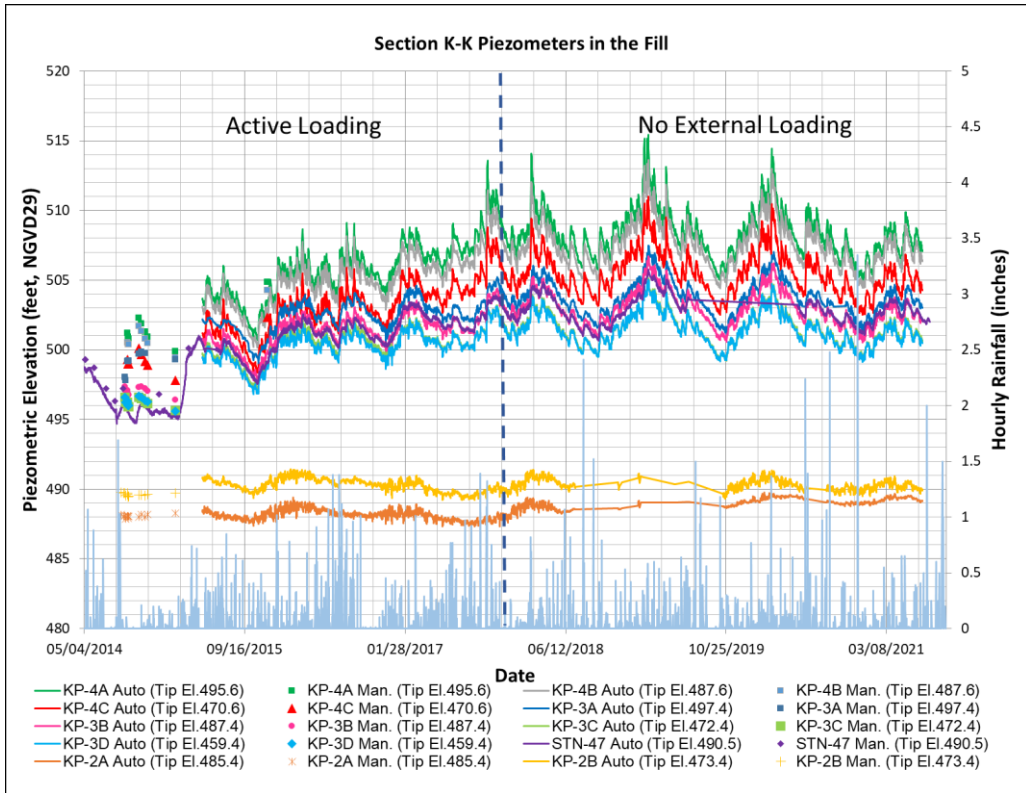
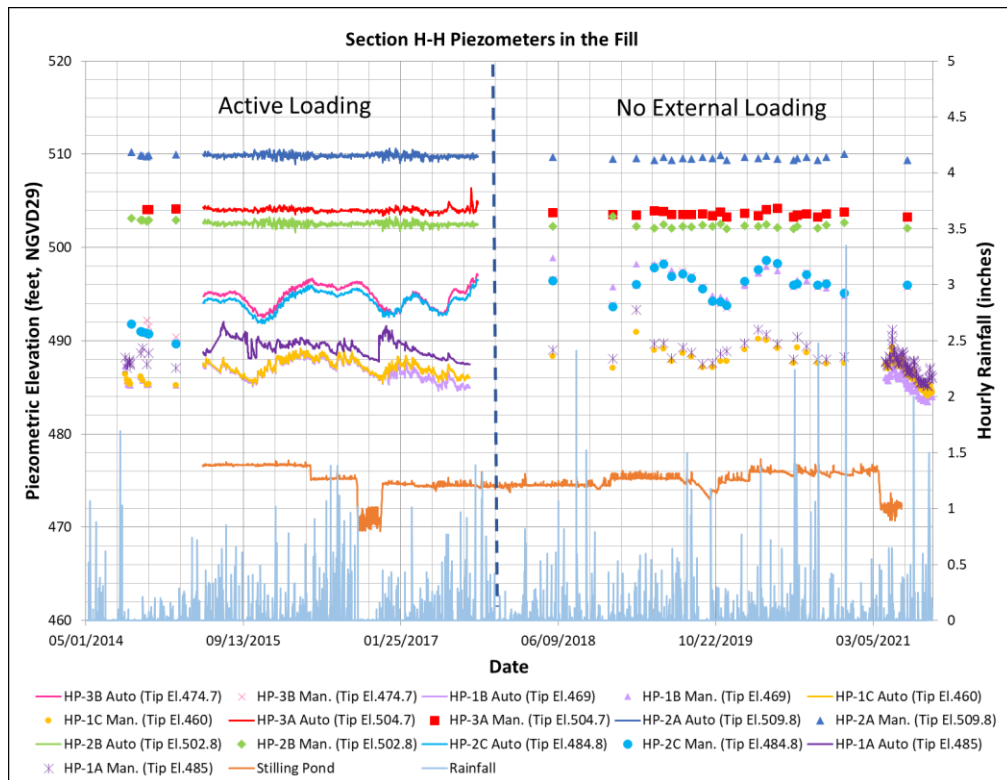Figure 36. Phreatic water levels within CCR Stack in West Pond

Figure 37. Phreatic water level within CCR Stack in East Pond

26

Readings of adjacent extensometers and inclinometers were paired to calculate displacement ratios at elevations where movement was observed. The displacement ratios were used to monitor the potential for shear induced lateral spreading and volumetric deformation of the gypsum and gypsum/fly ash due to changes on effective stresses within the fill. The results of this review are presented in the following sections.
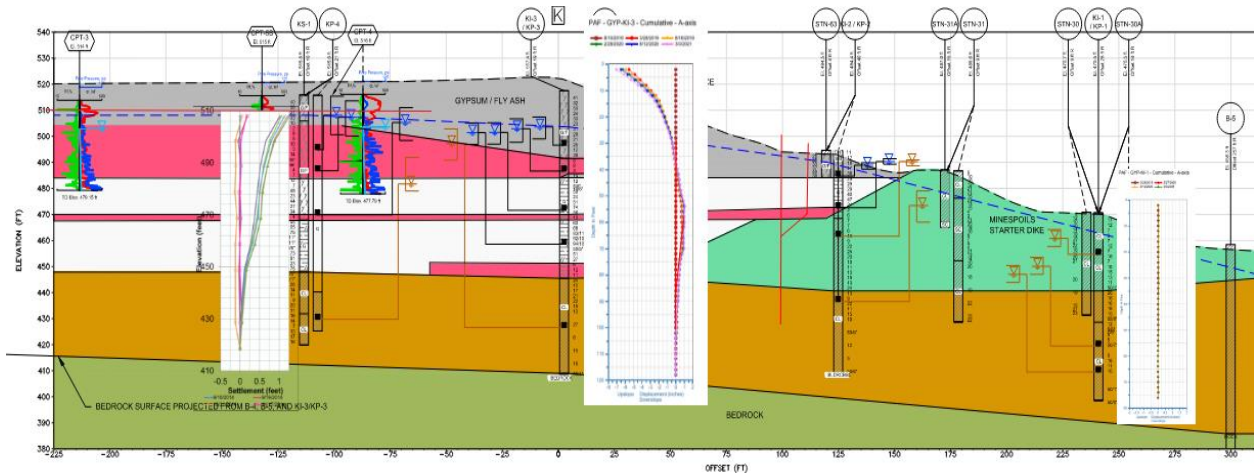
WEST POND

Figure 38. Representative cross section of the West Pond with instrumentation plots.

Figure 38 presents a cross section of Section K-K at the West Pond with the extensometers and inclinometer plots in their corresponding locations. There is one Sondex settlement system (KS-1) and two active inclinometers (KI-1 and KI-3) to monitor deformations on the West Pond. Inclinometer KI-3 is located at the top of the stack near the edge and KI-1 is located at the starter dike bench. The Sondex KS-1 is located at the top of the stack. A zone of lower strength material was identified at Section K-K from about El. 467 to 470.
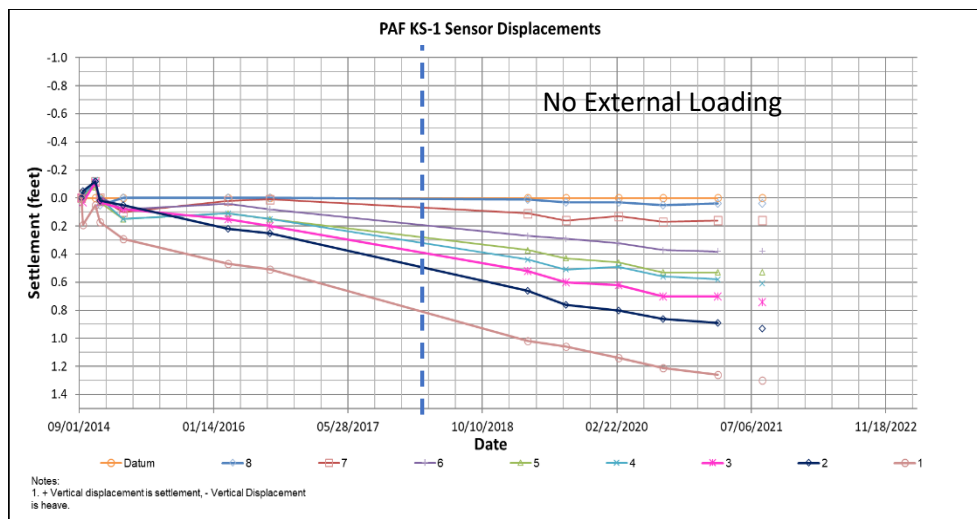
Vertical Displacement

Figure 39. Record of vertical deformation at West Pond.

Figure 39 shows the vertical settlement recorded in the West Pond from 2014 until 2021. It should be noted that settlement continued after the end of 2017, even though there were not external loadings applied to the west pond stack.
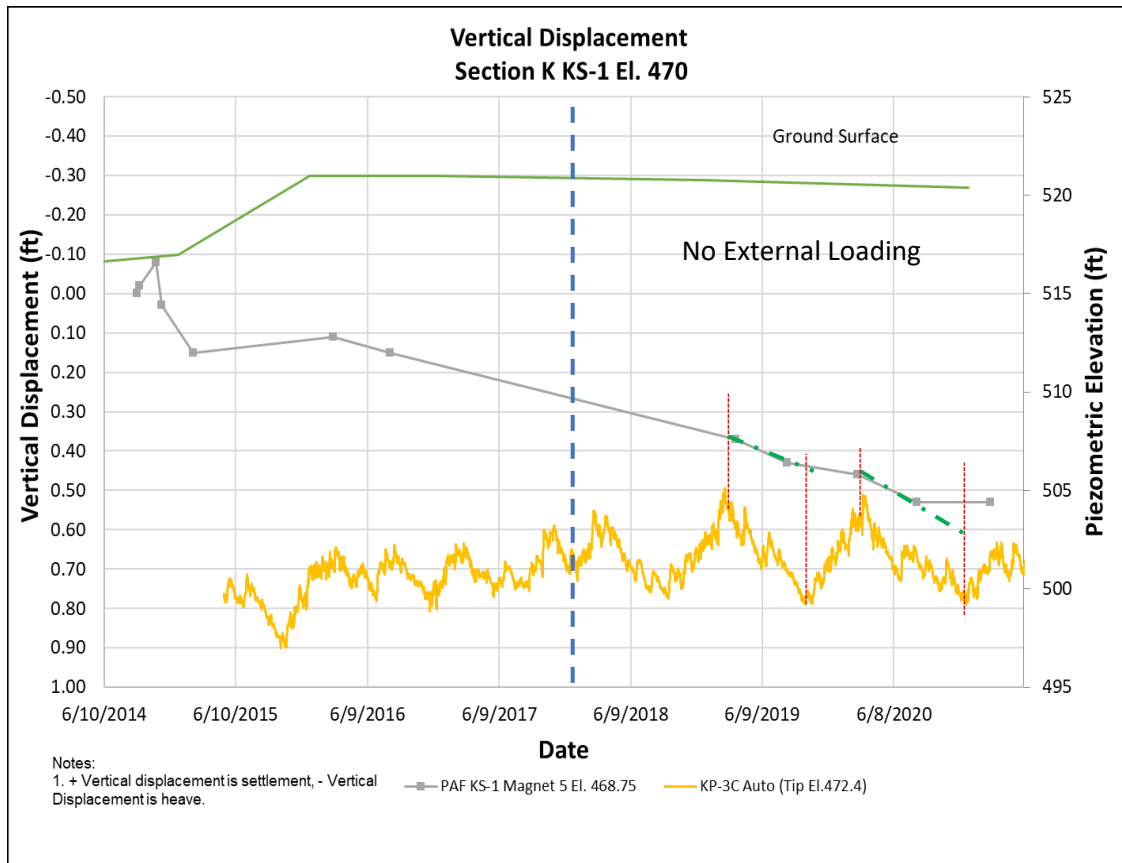

Figure 40. Cumulative vertical displacement and associated phreatic level at layer of interest, approximately elevation 470.

The Sondex KS-1 extensometer revealed an increase in vertical settlements at approximate El. 470 located in the identified lower strength zone, as shown in Figure 40. After the end of 2017, when active loading ceased, higher rates of vertical displacement were experienced during periods when lowering phreatic level trends (and therefore higher vertical effective stresses) occurred.

Lateral Displacement

Inclinometer KI-1 located at the toe of the berm shows very little to no movement after 2018. Inclinometer KI-3 shows upslope movement towards the top of the inclinometer and downslope movement at depth between 55 ft and 70 ft (El. 475 to El. 460). The shape of the cumulative displacement plot for KI-3 is typical of horizontal movement related to consolidation settlement. The downslope movement coincides with the lower strength zone identified in the section.
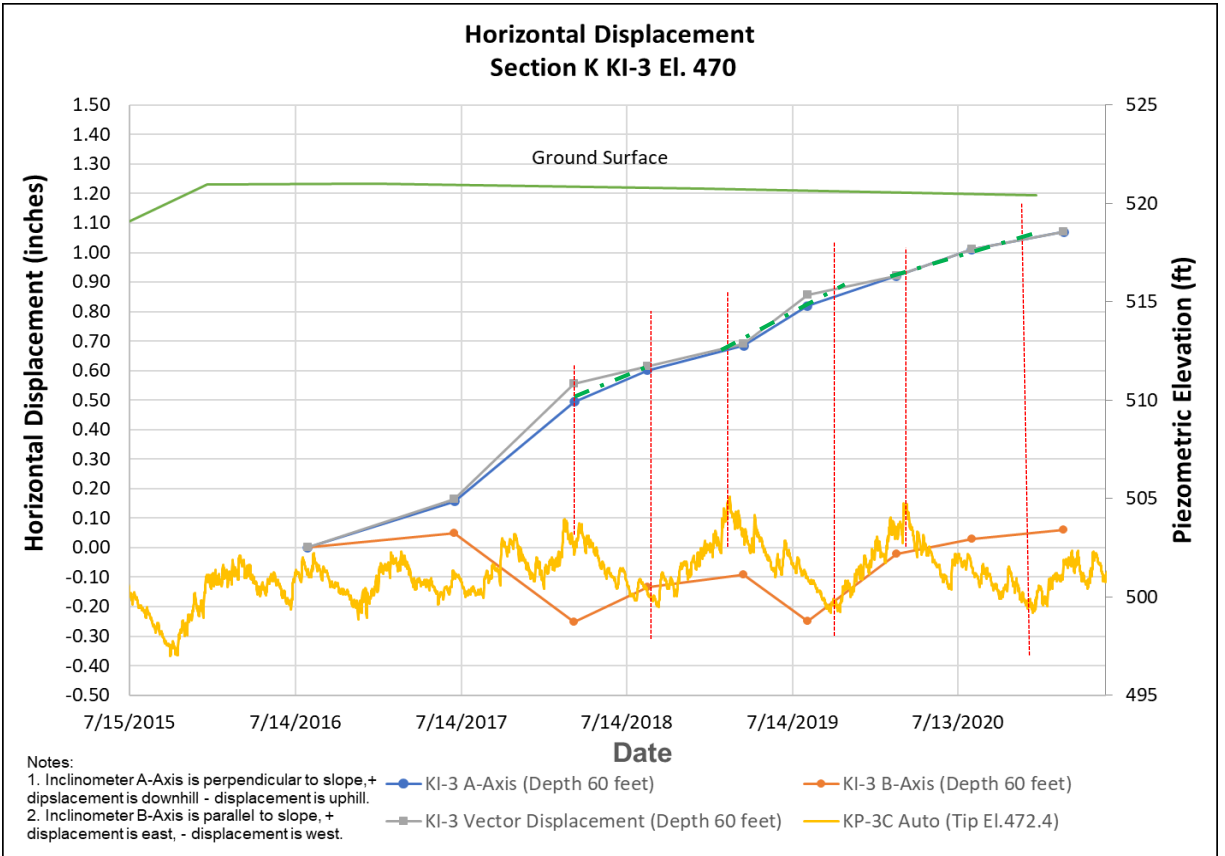
28

Figure 41. Cumulative horizontal displacement and associated phreatic level at layer of interest, approximately elevation 470.

The plots of horizontal and vertical displacements at El. 470 with pore water pressures from adjacent piezometer KP-3C show a trend of increasing movements in both horizontal and vertical directions when pore water pressures decrease, as shown in Figure 41. The decrease in pore water pressures causes an increase in effective stresses, providing the loading that results in additional settlement and lateral movement. After the end of 2017, when active loading ceased, higher rates of lateral displacement were experienced during periods when lowering phreatic level trends were being achieved.

Soft foundations may experience long-term lateral displacements several times larger than what may be measured at the end of construction, and although the mechanisms causing this phenomenon are unclear, Ladd (1991) indicated that in his opinion an important causal factor of the continued shear distortions is "undrained" creep. To develop and understanding of the nature of movements at Section K-K', the deformation ratio at El. 470 was calculated using lateral movements from readings of inclinometer KI-3 and vertical movement from readings of extensometer KS-1. A plot of displacement ratio versus time is shown in Figure 42. Displacement ratios in each direction as well as the resultant "vector" ratio are shown.
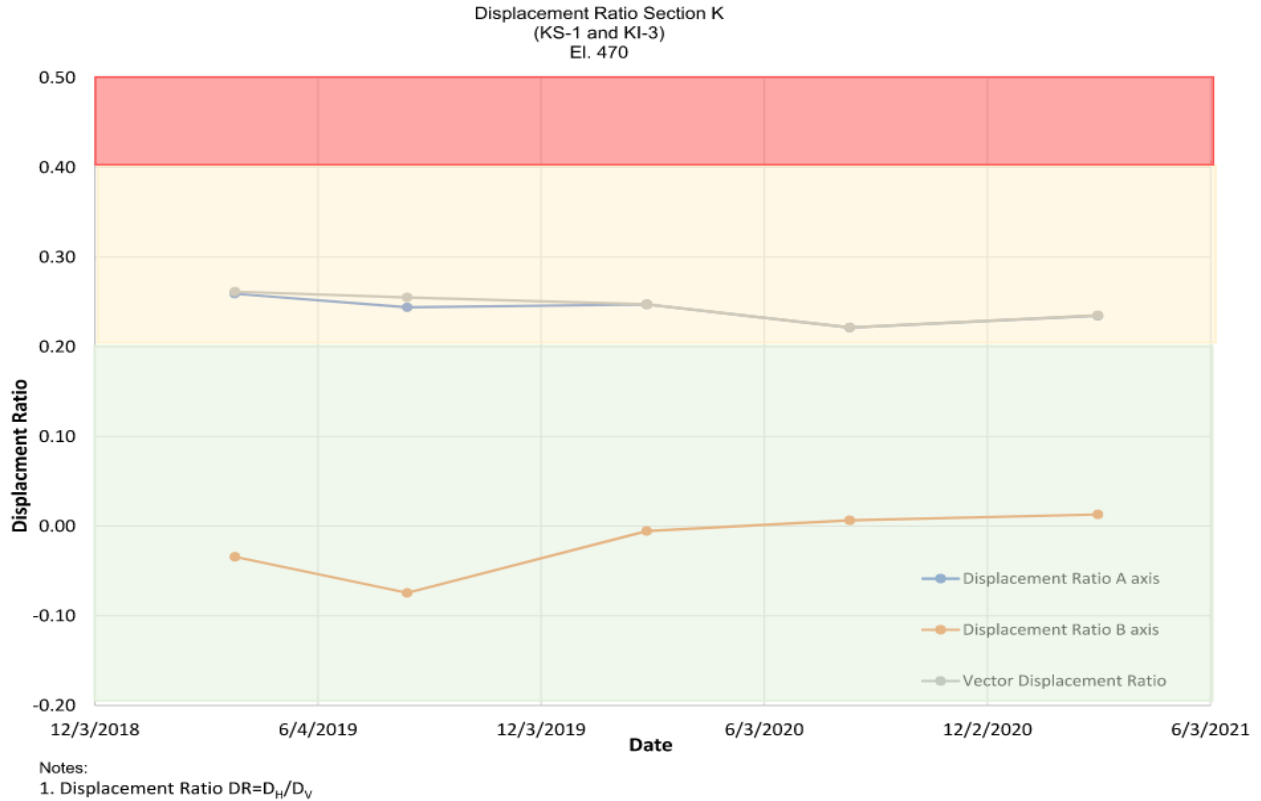
29

Figure 42. Displacement Ratio versus time at layer of interest, approximately elevation 470.

The maximum displacement ratio from 2019 to 2021 ranges from 0.22 to 0.26 and generally remains stable. Even though the displacement ratios are slightly above 0.2, they are relatively stable and do not appear to increase with time.

During closure, the stack is going to be re-graded and capped and rainwater infiltration will be cut off. Therefore, it is expected that the piezometric elevation within the stack will decrease significantly. These processes will cause an increase in effective stress leading to additional potential vertical and lateral movements.

EAST POND

Figure 43 shows a representative cross section of the East Pond with inclinometer and extensometer results plotted at their corresponding locations. There are two extensometers HE-1 and HE-2, one active inclinometer HI-1, and one inactive inclinometer HI-2 at Section H-H. Inclinometer HI-2 is located at the top of the stack near the edge of the slope and HI-1 is located at the stack bench. Extensometers HE-1 and HE-2 are located at the top of the stack; HE-2 is installed in the same borehole as HI-2.
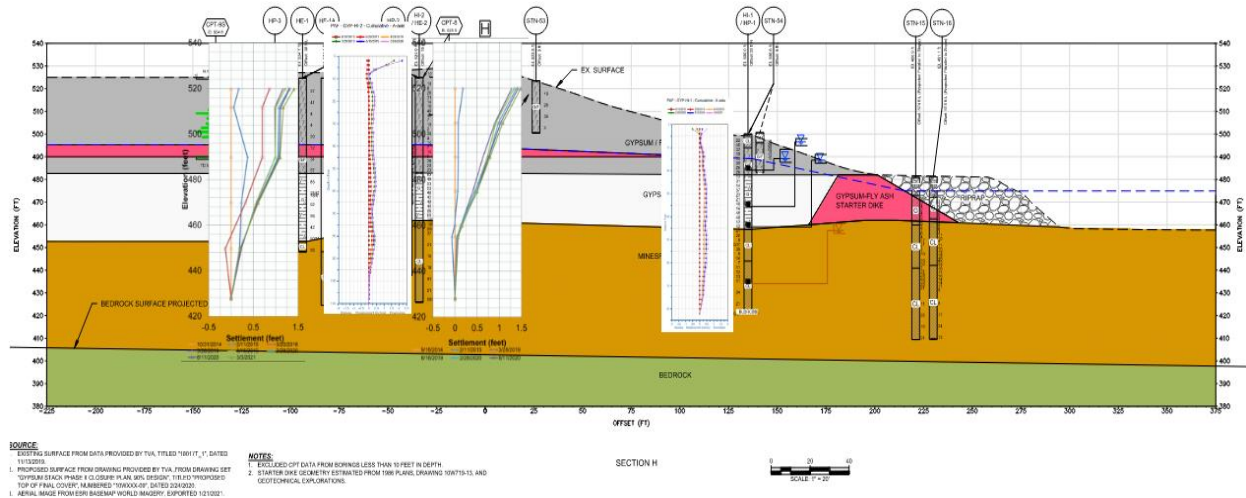
Figure 43. Representative cross section of the East Pond.

A zone of lower strength material between El. 490 and El. 495 was identified at Section H-H. To evaluate movements at Section H-H the readings from extensometer HE-2 and HI-1 were compared. Inclinometer HI-1 showed consistent movement from 2016 until the latest readings in 2021. From the cumulative displacement plot, two zones of large lateral displacement were identified. The first large displacement zone is located at a depth of 14 ft (El. 490), which corresponds to a lower-strength material zone at Section H-H. The second large displacement zone was located between depths of 24 and 40 ft (El. 480 and El. 466).   Vertical displacements are plotted in Figures 46 and 47, and horizontal displacements are plotted in Figures 46 and 47
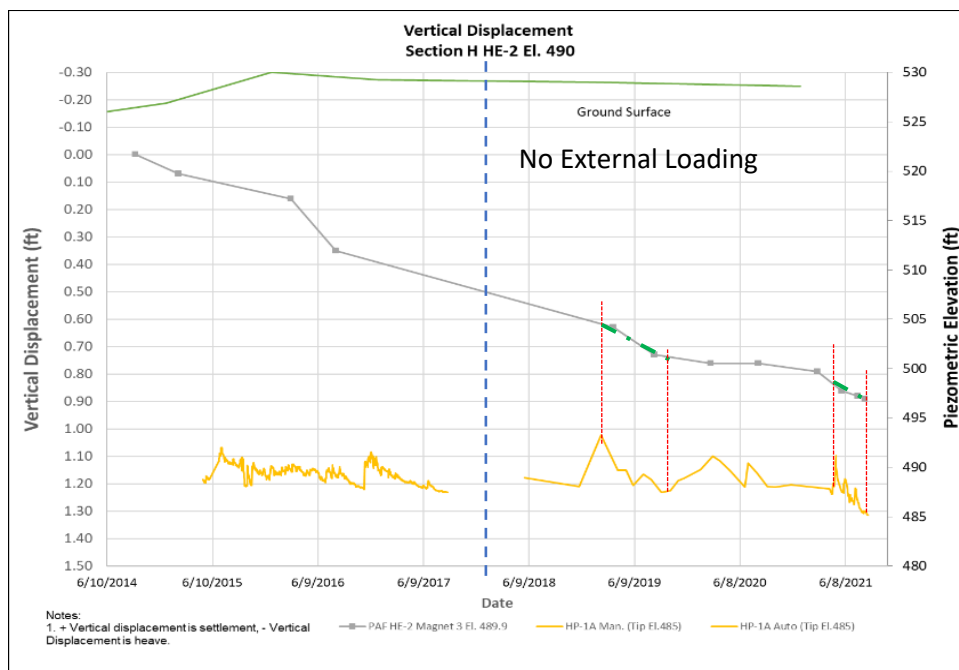Water levels in corresponding piezometers are shown in all four figures

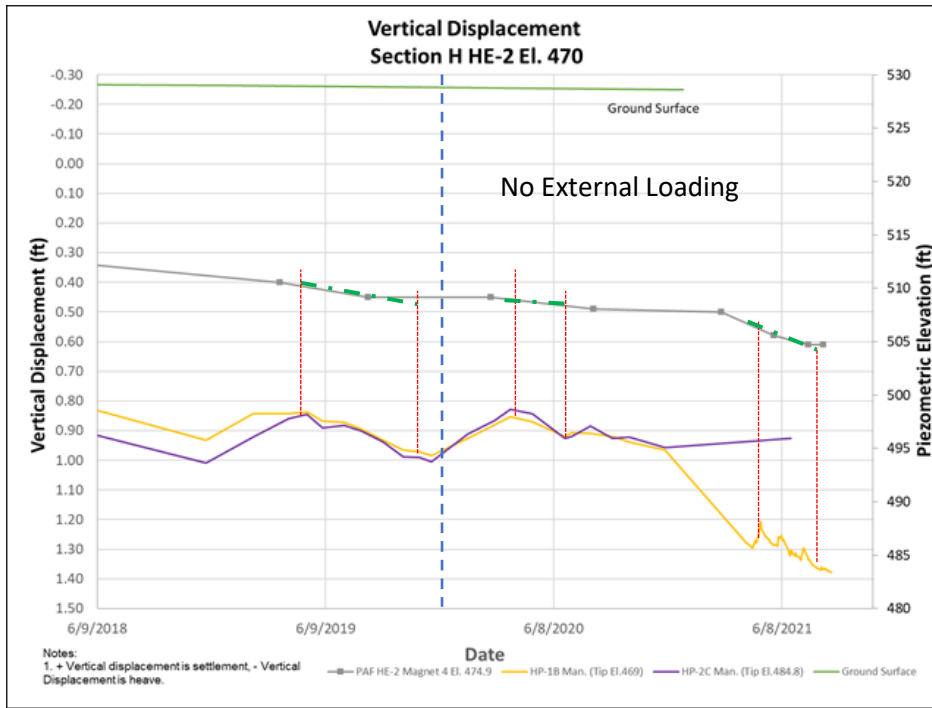Figure 44. Vertical displacement at elevation 490.

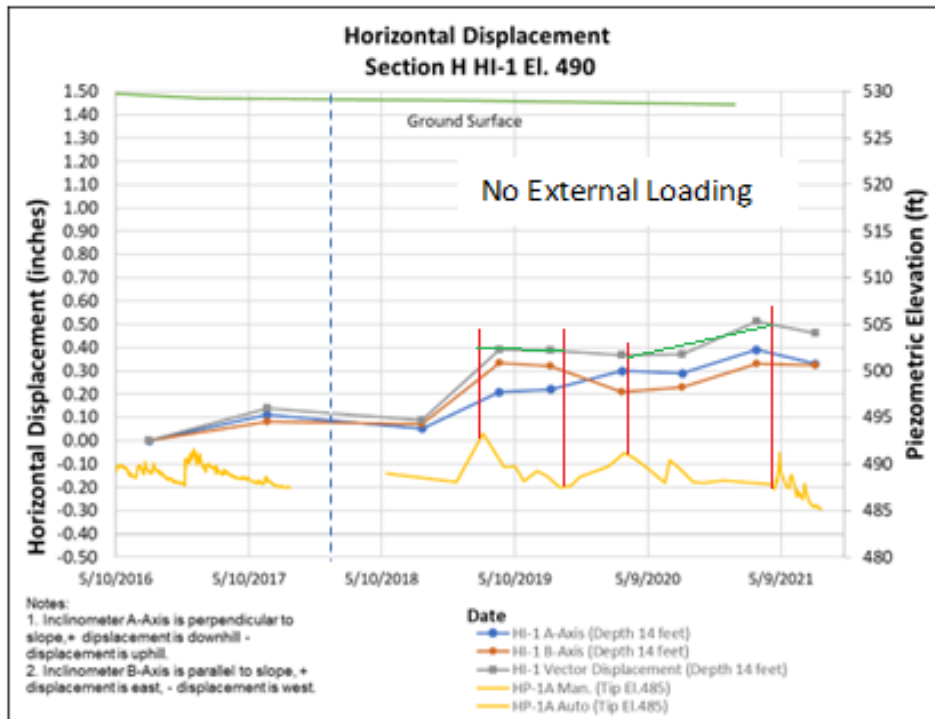Figure 45. Vertical displacement at elevation 470.

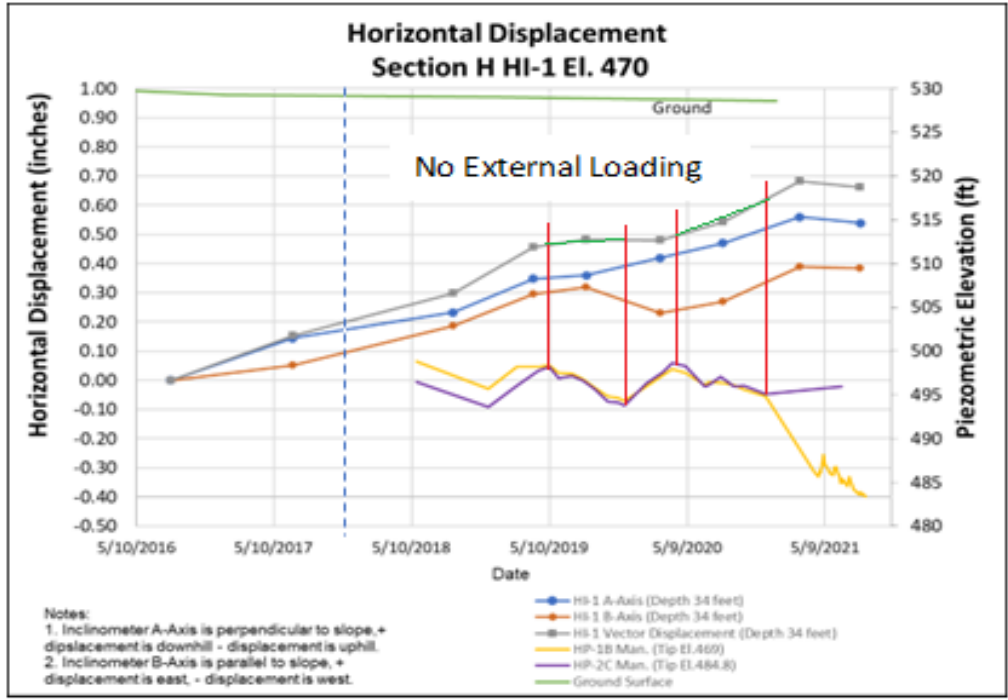Figure 46. Horizontal displacement at elevation 490

Figure 47. Horizontal displacement at elevation 470

The plots in Figures 44 through 47 reveal a trend of increasing movements in both horizontal and vertical directions when pore water pressures decrease. The decrease in pore water pressures cause an increase in effective stresses in the soil, which results in additional settlement and lateral movement. Deformation ratios at El. 490 and El. 470 were determined using lateral movement at depth, from readings of inclinometer HI-1, and vertical movement, from readings of HE-2. The deformation Ratios are plotted in Figures 48 and 49.
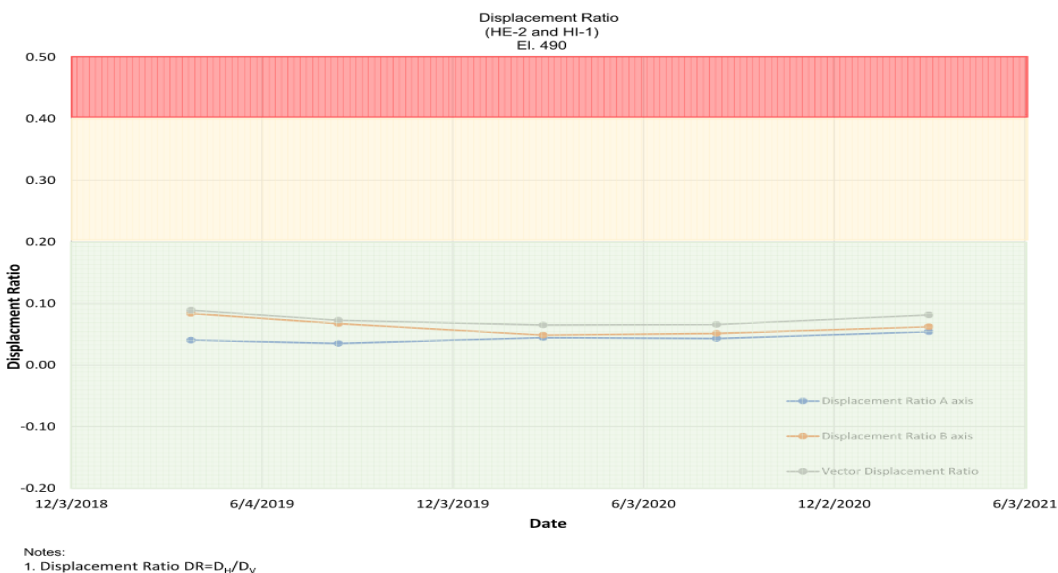

Notes:
1. Displacement Ratio DR=D_H/D_V

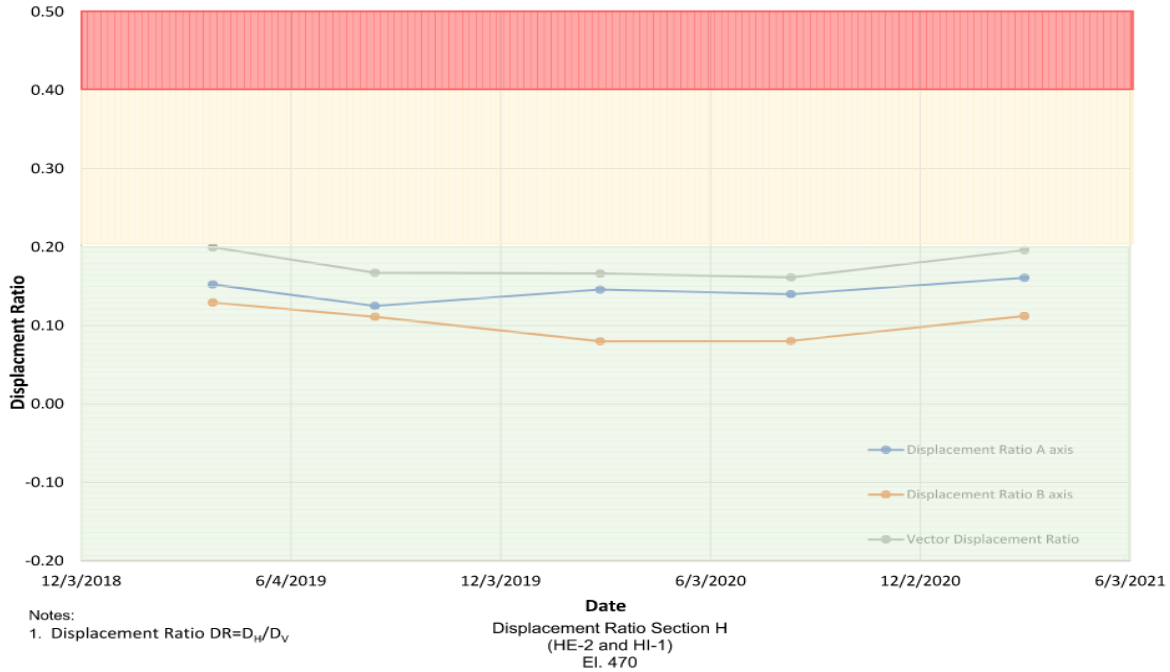Figure 48. Displacement Ratio at Elevation 490.

Figure 49. Displacement Ratio at Elevation 470

At El. 490 the displacement ratio remained at low levels, ranging from 0.06 and 0.09. At El. 470 the displacement ratio ranged between 0.16 and 0.2, and generally remains stable. The maximum displacement is equal to 0.2, which indicates consolidation behavior of the stack. However, an increasing trend in displacement ratio was observed when plotting the last set of readings of these instruments.

Based on a review and analysis of the instrumentation data, the facility appears to be stable. There are no visible signs of instability and active stacking has not taken place since 2017. Movements observed in the inclinometers and extensometers are consistent with consolidation behavior of the stack, and the development of drained conditions. Settlement under fill load is still ongoing, especially in the soft CCR layers. Vertical and lateral movements increase when the phreatic level drops, indicating that increasing effective stresses in the stack cause additional consolidation of the softer materials. Increasing trends on the deformation ratio warrants continued monitoring of the movements at this facility as an indicator of its performance.

Comparison of Field Performance and Laboratory test Results

Closing of facilities general results in preventing or limiting infiltration of water and therefore a lowering of the phreatic level overtime. As the phreatic level drops over time, the effective stress on layers of interest will increase. To determine if these increases are resulting on detrimental behavior to the facility or to its appurtenances, one may compare the field deformation behavior of the weak CCR deposits with the behavior of the material observed in laboratory tests. A plot of the values of the deformation ratio versus incremental effective vertical stress from a triaxial test, shown in Figure 50, can be used to guide the understanding of the movements as the facility's long-term behavior is monitored.
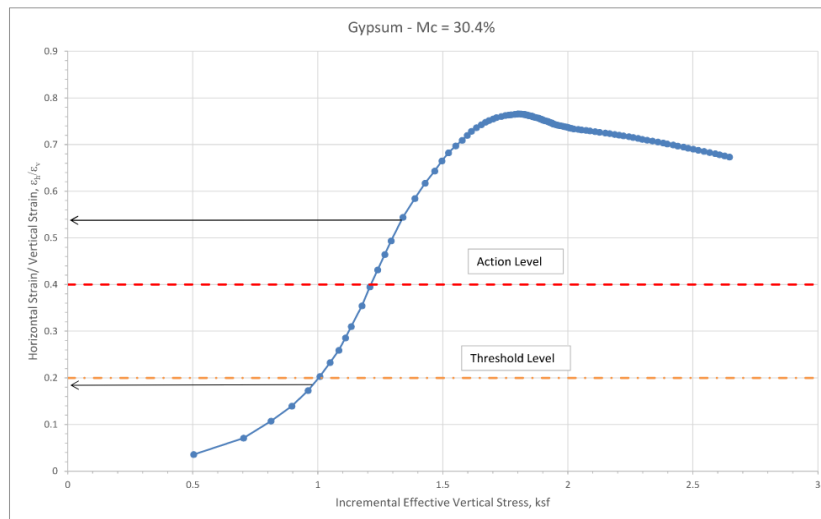
Figure 50. Deformation Ratio vs effective vertical stress during Triaxial CU' test.

V - CONCLUSIONS

A framework for monitoring the performance of constructions over soft or weak CCR deposits has been presented. The framework can be used to monitor the performance of a CCR facility during the construction process, throughout the service life, and for a prudent post closure period .

The applicability of using deformations to monitor short- and long-term performance of CCR facilities was presented for two common scenarios of construction over soft, saturated CCR deposits.

The proposed framework supports the post-closure monitoring of closed facilities. Closing CCR facilities generally results in preventing or limiting infiltration of water and therefore a lowering of the phreatic level overtime. The lowering of the phreatic level increases the effective loading leading to deformation of soft or weak layers within CCR deposits.

The authors suggest establishing threshold and action levels for deformation parameters based on an understanding of the stress-strain behavior of the materials of interest during laboratory testing.

The authors also suggest that comparisons between the field data and the laboratory data be considered, for the relationships of interest, during the monitoring period to ascertain that the facility is performing as expected during its design**.**

Ultimately, the authors believe that the proposed framework to monitor the performance of CCR facilities will provide consisting indication of behaviors that may bring a potential impending failure to the facility, allowing for intervening actions in a timely fashion to prevent significant consequences.

REFERENCES

Bozok, O., Sabatini, P.J., and Amaya, P.J. ,*Use of Instrumented Test Fill to Assess Static Liquefaction of impounded Fly Ash*, , 2013 World of Coal Ash Conference, Lexington, KY.

El-Ramley, *Probabilistic analysis of landslide hazards and risks: bridging theory and practice*. PhD Thesis. 2001.

EPRI, "*Geotechnical Centrifuge Tests to Assess Stability of Slurry-Deposited Coal Fly Ash: Runout and Dewatering Behavior Analysis."* Palo Alto, CA: 2021. 3002020566.

Hunter, G., and Fell, R., *Prediction of impending failure of embankments on soft ground*, Canadian Geotechnical Journal, 40, 209-220, 2003

Loganathan, N., Balasubramaniam, A. S., Bergado, D. T., *Deformation Analysis of Embankments*. Journal of Geotechnical Engineering, Vol. 119, No. 8 August 1993

Ladd, C. C., *Stability Evaluation During Stage Construction*, The Twenty-Second Karl Terzaghi Lecture*,* Journal of Geotechnical Engineering, April 1991

"Soil Mechanics". T. William Lambe, and Robert Whitman. John Wiley and Sons, Inc. New York, NY. 1969.

Tavenas, F., Mieussens, C., and Bourges, F.*, Lateral displacements in clay foundations under embankments.,* Canadian Geotechnical Journal, 16, 532 – 550, 1979.

Tavenas, F., and Leroueil, S., *The behavior of embankments on clay foundations*, Canadian Geotechnical Journal, 17, 236-260. 1980.

Walton, W., *Personal communication,* October 24, 2017.